GSJ: Volume 10, Issue 5, May 2022, Online: ISSN 2320-9186
www.globalscientificjournal.com

SIMULATION OF QUANTUM TUNNELLING IN A MODIFIED WOODS-SAXON POTENTIAL BARRIER

[1]Ormin Bundega Joseph, [2]Idugba Mathias Echi

[1]Department of Science Laboratory Technology, School of Science and Technology, Federal Polytechnic Bali, Taraba State, Nigeria. Email: orminjoseph@gmail.com
[2]Department of Physics, College of Science, Joseph Sawuan Tarka University, Makurdi, Benue State, Nigeria. Email:

KeyWords

Quantum mechanics, Schrodinger equation, Tunneling effect, nuclear reaction, finite difference method, Woods-Saxon potential, current density, neutron-nucleus interaction, elastic and inelastic scattering.

ABSTRACT

In this paper, quantum tunneling phenomena is simulated in the $\mathrm{neutron}$ – Fe-56 interaction using a modified Woods-Saxon potential. The one-dimensional Schrödinger equation is numerically solved using finite difference method implemented with Jacobi transformations in order to satisfy the boundary conditions. The standard Woods-Saxon potential parameters were kept constant at $W_0 = 50\,\mathrm{MeV}$, $a = 0.65\,\mathrm{fm}$, $V_0 = 47.78\,\mathrm{MeV}$ and $R_0 = 4.9162\,\mathrm{fm}$ respectively. The wavefunctions and the transmission coefficients of the neutrons as it tunnels through the Fe-56 nuclide with different angular momenta $l = 0, 1, 2, 3, 4$ and various energies of the projected neutron were obtained. The simulation algorithm is coded in MATLAB computer language. The results obtained show that the projected neutron can tunnel through the barrier even when the energies of the projected neutron are less than the energy of the barrier. For neutron with purely translational kinetic energy ($l = 0$), it is observed that after tunneling there is no attenuation or reduction in its intensity and amplitude after interacting with the Fe-56 nucleus, indicating perfect tunneling and transmission of the neutron through the Fe-56 barrier. At other angular momenta (i.e., l=1,2, 3…) the wavefunction of the transmitted neutron attenuates after tunneling, with a change in amplitude as it tunnels through the barrier. Further results show that the transmission coefficient attains saturation at an incident energy approximately equal to $E_s = -0.1309\,\mathrm{eV}$. The E_s value may serve as an experimental guide (given the barrier parameters) in neutron-Fe-56 scattering experiments particularly in elastic regime. It is recommended that further research be carried out using other target nuclei as this could significantly contribute to a better knowledge of tunneling probabilities for neutron-nucleus or nucleus-nucleus interactions.

I. Introduction

Quantum tunneling refers to the transmission of microscopic particles through any arbitrary barrier with energy less than the barrier height. The tunneling effect is one of the most significant distinctions between classical and quantum mechanics. Classically, it is known that when a particle which has an energy E (which is always non-negative), encounters a potential barrier, $V(r)$ then, the particle simply cannot be located at a point r ($r > 0$) with the potential barrier greater than the energy of the particle ($V(r) > E$). However, quantum mechanically, a particle which has a definite value of energy, E, on encountering a potential barrier has a non-zero probability of being located in the classically forbidden region [6] [13] [23] [28] [30].

The study of radioactivity which was discovered in 1896 by Henri Becquerel ushered in the development of quantum tunneling. It was found that the emission of particles and energy from the unstable nucleus of an atom to form a stable product is as a result of tunneling of the particle out of the nucleus. Its first application was a mathematical explanation for alpha decay, which was developed in 1928 by George Gamow [20].

In recent years, tunneling has been a great breakthrough most especially in the demand in high-speed and new functional device applications. It is widely applied in modern devices and modern experimental techniques, such as the tunnel diode (in electrical semiconductor devices when heavily doped), the scanning tunneling microscope (in imagining the surface of a conductor), quantum biology (in many biochemical redox reactions such as photosynthesis, cellular respiration as well as enzymatic catalysis and in spontaneous DNA mutation), nuclear fusion (where tunneling increases the probability of atomic nuclei to overcome the coulomb barrier in stars' core to achieve thermonuclear fusion) among others [11] [35].

The application of interest for this paper is to investigate quantum tunneling in the nuclear reaction of neutron-Fe-56 interaction. Neutrons by virtue of being neutral particles can approach a target nucleus without any interference from a Coulomb repulsive or attractive force. Once in close proximity to the target nucleus, neutrons can interact with the nucleus through the short range attractive nuclear potential and trigger various nuclear reactions. The study of the neutron-nucleus has motivated a lot of researchers for the fact that the neutron can represent a significant source of indirectly ionizing radiation along its path as it interacts with various nuclei.

Furthermore, the neutron is quite sensitive to light atoms like hydrogen, Oxygen, etc. which have much higher interaction probability as compared to metals. Since the neutron is electrically neutral, it interacts only weakly with matter into which it can penetrate deeply. Metals comparatively show lower interaction probability with neutrons, thus allowing quite high penetration depth [9].

The interaction of neutron-Fe-56 is a nuclear process in which the neutron and Fe-56 collide to produce one or more nuclides (isotopes) with a release of an enormous amount of energy. This interaction results in so many processes depending on the energy possessed by the neutron and the nature of Fe-56 which can lead to either absorption or scattering of the neutron by Fe-56 [15] [16]. When the neutron is absorbed by Fe-56, the resulting isotope is in its excited state. At some point in time, the heavy isotope will split into two or smaller isotopes called the fission fragments mostly of unequal masses. This absorption could be electromagnetic absorption (involves photons or higher energy photons such as gamma rays being emitted), charged particle absorption (involves the iron-56 emitting different types of radiations, like ∝-particles orβ-particles), neutral absorption (involves the Fe-56 emitting another neutron from the Fe-56 nucleus) and fission. Scattering of the neutron as it collides with the Fe-56 could be elastic or inelastic scattering. In elastic scattering, there is no transfer of energy between the neutron and the Fe-56. As the neutron collides with the Fe-56 and share part of its kinetic energy, they are then repelled with speeds different from the original speeds such that the total kinetic energy between the two particles is conserved. The collision emits an Fe-56 which is in its ground state and a single neutron. In the case of inelastic scattering, as the neutron interacts with the Fe-56, the Fe-56 goes into an excited state due to the momentum energy that the incoming neutron had and at later point in time, the Fe-56 will emit some radiation due to de-excitation.

To describe neutron-nucleus interaction and nuclear reaction dynamics, the knowledge of the potential between the two colliding particles is of fundamental importance. Notable equations for radius-centered potentials in recent years has attracted many researchers, such as the Rosen-Morse potential, the Morse potential, the Yukawa potential, Woods-Saxon potential among others [27]. The Woods-Saxon potential has attracted a great deal of interest over the years and has been one of the most useful models for determining the single particle energy levels of nuclei and the nucleus-nucleus interactions. The Woods-Saxon potential was first proposed by R.D. Woods and D.S. Saxon in 1954 to describe the elastic scattering of 20 MeV protons on heavy nuclei [3] [4] [7] [21] [26] [27]. The Woods-Saxon potential is a well-known potential and one of the most realistic short-range potentials in physics which is considered in the present paper to describe the quantum tunneling behavior of the neutron as it interacts with the Fe-56. Figure 2 illustrates various possibility outcome of neutron- $Fe-56$ interactions.

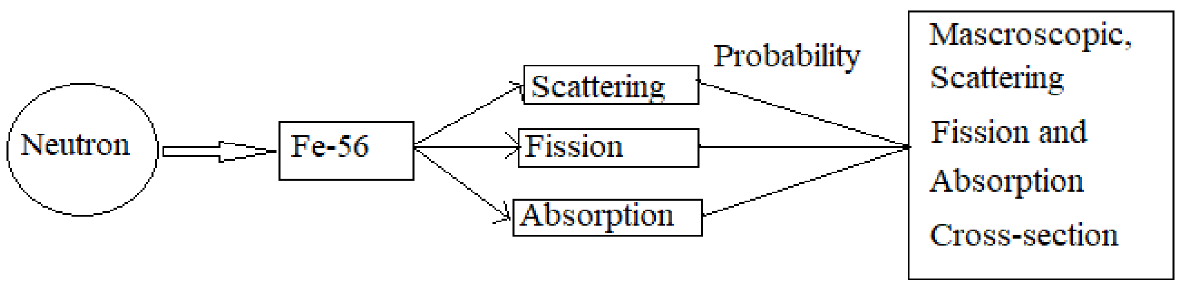

Figure 1: Schematic of various interactions of a neutron with Nucleus.

In order to find out how a particle can tunnel through a physical system; a potential model is considered and then the Schrodinger equation is solved to find the appropriate wavefunctions [8] [18][33].

The radial part of Schrödinger equation numerically for the Woods-Saxon potential, the general Woods-Saxon potential, and D-dimensional Woods-Saxon potential was solved in [24] by applying finite difference method and Jacobi method to investigate the interaction of neutron with Fe-56. The eigenvalues which are energies of the eigensystem and the eigenvectors which are related to the wave functions were obtained.

Also, the angular distributions of the C-12 elastic scattering from K-39, Ca-40, Fe-56, Ni-64, Zr-90;91;92;94;96, In-115, Sn-116;117;118;119;120;122;124, Tm-169 and Bi-209 with incident energies between 4.5 and 35 MeV was experimented in [21]. The optical potential parameters were analyzed. The systematic Woods-Saxon potential parameters were also presented and then tested by the comparison between the calculation results and the experimental angular distributions of the heavy-ion elastic scattering.

The likelihood of neutron-nucleus (Fe-56) interaction has been well covered in the literature over the decades in terms of its cross section [19] [21]. Also, the eigenvalues and the corresponding eigenfunctions have been solved for some neutron-nucleus and nucleus-nucleus interactions in the literature [2] [3] [4] [14] [17] [22] [24] [25] [29] [30]. However, transmission probability which shows the tendency of a neutron's current flux penetrating the potential barrier in a Fe-56 nucleus has not been given adequate attention in the literature. Therefore, there is a great deal of analysis on transmission probability, which includes the ability of the neutron current flux to tunnel through the potential barrier in the Fe-56 nucleus along the boundaries. The theory developed in this paper takes a more general approach, which avoids many simplifications previously imposed to calculate the probability current density. Also, this paper evolves a computational approach previously used to calculate the eigenfunctions with the application of finite difference method and Jacobi transformation.

Additionally, the theory of quantum tunneling has been so limited to problem which can be solved analytically. It becomes a simple procedure to match solutions at the boundary and extract the transmission coefficients as ratio of transmitted and incident probability currents. Where the potential barrier is such that analytic solutions are not possible as in the modified Woods-Saxon potential there is no simple way to extract transmission coefficients. The free particle region solution is assigned a wave function a priori and evaluated at the boundary. In this work, we employed a numerical technique that solves the problem in the potential region at the same time matching the solution at the boundary to the free particle solution to avoid discontinuity of the solutions.

Figure 2 illustrates the scattering of the neutron wavefunction as it interacts with the potential barrier ($Fe-56$).

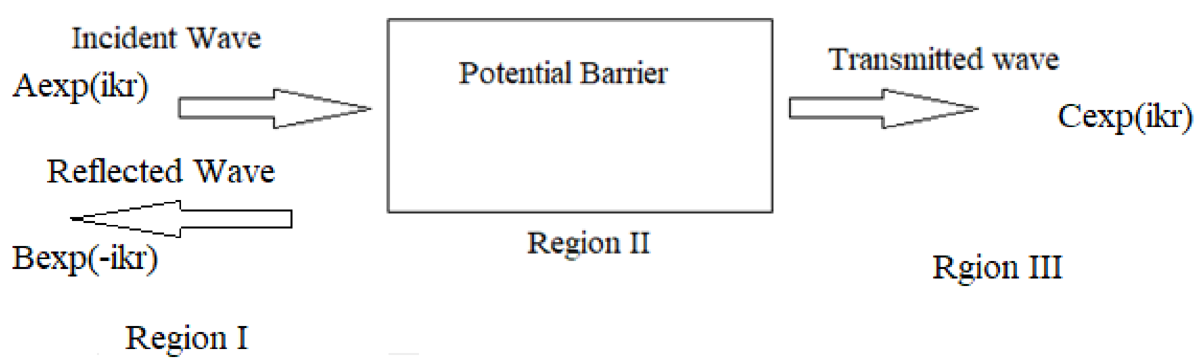

Figure 2: Neutron-Fe-56 interaction

This paper is organized as follows: the finite difference method, the Jacobi method, the Woods-Saxon Potential are presented in section II. The radial part of the Schrodinger equation with the modified Woods-Saxon Potential and its solution are also presented in this section. Numerical results and detailed discussions are given in section III and IV respectively. Summary and conclusion are presented in section V.

II. Theoretical Consideration

A. Finite Difference Method

The finite difference method is one of the methods used in discretization of differential equations. The FDM subdivides the simulation domain into small segments, called step size. Each step size boundary is called a node and the unknown variables are defined on these nodes. The derivatives in the differential equation to be solved are replaced by discretized finite difference approximations at each one of the nodes. These approximations may be derived from a truncated Taylor series. From Taylor series expansion, it is assumed that if a function $f\ (x)$ is a continuous, single-valued function with continuous derivatives, then [5] [[31].

$$f\ (x + \Delta x) = f\ (x) + \Delta x f^{'}\ (x) + \frac{\Delta x^2}{2!} f^{''}\ (x) + \cdots, \qquad (1)$$

$$f\ (x - \Delta x) = f\ (x) - \Delta x f^{'}\ (x) + \frac{\Delta x^2}{2!} f^{''}\ (x) - \cdots, \qquad (2)$$

where Δx is the step size. This discretization provides second-order accuracy with a local truncation of $o(\Delta x)^2$. The approximation is:

$$f^{'}\ (x) = \frac{f\ (x+\Delta x) - f\ (x)}{\Delta x} \qquad (3)$$

$$f^{''}\ (x) = \frac{\frac{f\ (x+\Delta x) - f\ (x)}{\Delta x} - \frac{f\ (x-\Delta x) - f\ (x)}{\Delta x}}{\Delta x} = \frac{f\ (x+\Delta x) - 2f\ (x) + f\ (x-\Delta x)}{(\Delta x)^2} \qquad (4)$$

This type of approximation is called central finite difference approximation. Other methods include; Transfer Matrix method and transmission line method [1] [10] [32].

B. Jacobi Method

This iterative method was first proposed by Carl Gustav Jacob Jacobi, in 1846, to calculate the eigenvalues and corresponding eigenvectors of a real symmetric matric or eigensystems of equations. The method uses similarity transformations on a given matrix. And after a sequence of these transformations, the matrix is converted into a diagonal matrix which corresponds to the eigenvalues. The sequence will also contain the information about the eigenvectors of the matrix. According to Carl Gustav Jacob Jacobi, if A is an $n \times n$ coefficients matrix, the diagonalized matrix of A is $A^{'}$ given as [12]:

$$J^T A J = A^{'} \qquad (5)$$

Multiplying with J on both sides gives:

$$AJ = JA^{'} \qquad (6)$$

$J = J_1 . J_2 . \ldots$ is an orthogonal matrix.

$$J = \begin{bmatrix} X_1 & X_2 & . & X_n \\ . & . & . & . \\ . & . & . & . \\ . & . & . & . \end{bmatrix} \text{ and } A^{'} = \begin{bmatrix} \lambda_1 & 0 & . & 0 \\ 0 & \lambda_2 & . & 0 \\ 0 & 0 & . & 0 \\ 0 & 0 & . & \lambda_n \end{bmatrix}$$

The Jacobi matrix is:

$$A \begin{bmatrix} X_n \\ . \\ . \\ . \end{bmatrix} = \lambda_n \begin{bmatrix} X_n \\ . \\ . \\ . \end{bmatrix} \qquad (7)$$

The columns of the Jacobi matrix give the eigenvectors, X_n of the matrix and the diagonal elements, λ_n are the eigenvalues.

C. Woods-Saxon type potential

The Woods-Saxon type potential for the wave equations such as Schrodinger equation are of high scientific importance in the conceptual understanding of the interactions between the nucleon and the nucleus. The modified version of the Woods-Saxon potential consists of the volume (standard) Woods-Saxon and its derivative called the Woods-Saxon surface potential and is given by [4].

$$V(r) = -\frac{V_0}{1+e^{\frac{r-R_0}{a}}} - \frac{W_0 e^{\frac{r-R_0}{a}}}{\left(1+e^{\frac{r-R_0}{a}}\right)^2} \qquad (a \ll R) \tag{8}$$

where V_0 and W_0 represent the depths of the potential well, R_0 and a are the radius of the potential and width of the surface diffuseness, respectively. The surface term in the generalized Woods-Saxon potential induces an extra potential pocket especially at the surface region of the potential and this pocket is so significant to explain the elastic scattering of some nuclear reactions. R, a and V_0 are also expressed as: [20]

$$R_i = 1.20 {A_i}^{1/3} - 0.9\, fm \qquad (i = P, T) \tag{9}$$

$$1/a = \left[1 + 0.53\left({A_P}^{-1/3} + {A_T}^{-1/3}\right)\right] fm^{-1} \text{ and}$$

$$V_o = (40.5 + 0.13 A_P)\, MeV$$

where A_P and A_T are the mass numbers of the projected and target nucleus respectively. The sketch of general Woods-Saxon potential is given in figure 3.

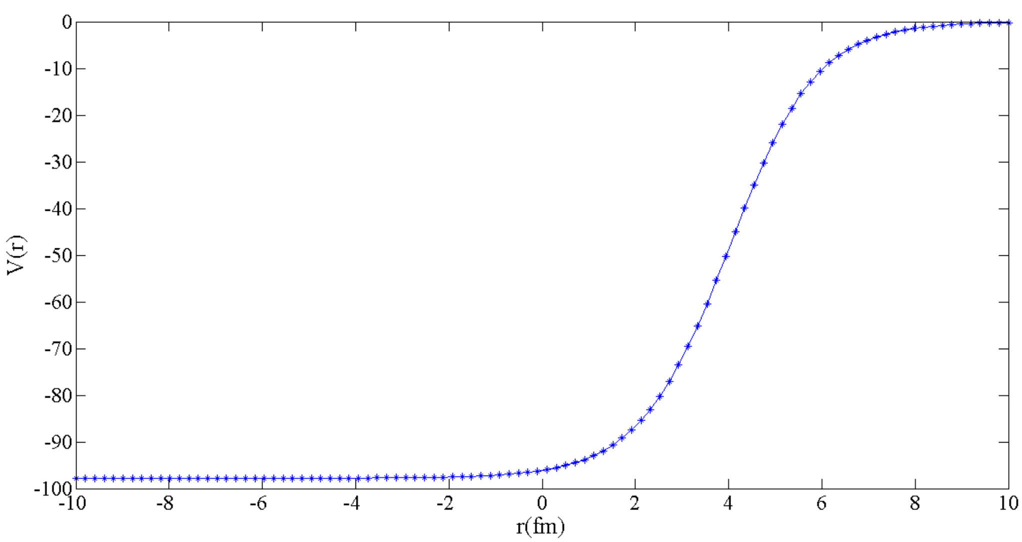

Figure 3: General Woods-Saxon potential for $W_0 = 50\ MeV, a = 0.65 fm, V_0 = 47.78\ MeV, R_0 = 4.9162 fm$ [17]

D. Modified Woods-Saxon Potential

For the modified Woods-Saxon Potential, we define the potential well describing the neutron-Fe-56 interaction as:

$$V_{mWS}(r) = -\frac{V_0}{1+e^{\frac{r-R_0}{a}}} + \frac{W_0 e^{\frac{r-R_0}{a}}}{\left(1+e^{\frac{r-R_0}{a}}\right)^2} \tag{10}$$

This modification will be used to describe the quasi-bound states in the nucleus, for $W_0 > 0$ [24]. Also, show the ability of a neutron with a certain energy penetrating through the modified potential.

where $A_n = 1.00866\ a.m.u$ and $A_{Fe} = 56.0\ a.m.u$ are the mass numbers of the neutron and $Fe - 56$ nucleus.

$a \approx 0.65 fm$ for mass number, $A \geq 40$. The sketch of the modified Woods-Saxon potential is shown in figure 4. It contrasts clearly with the general Woods-Saxon potential of figure 3.

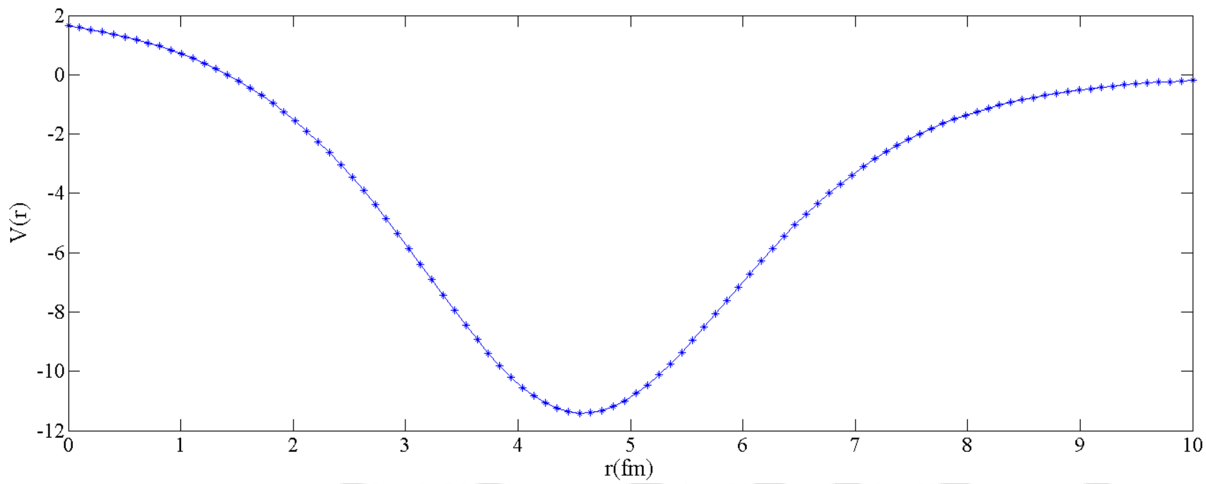

Figure 4: Modified Woods-Saxon potential for $W_0 = 50\ MeV, a = 0.65\ fm, V_0 = 47.78\ MeV, R_0 = 4.9162\ fm$

E. The radial part of Schrodinger Equation

The radial part of the Schrodinger equation which contains the modified Woods-Saxon potential and the repulsive potential (centrifugal potential) is given by:

$$\left[\frac{d^2}{dr^2} + \frac{2}{r}\frac{d}{dr} + \frac{2\mu}{\hbar^2}\left(E_{n,l} + V_{mWS}(r)\right) - \frac{l(l+1)}{r^2}\right] R_{n,l}(r) = 0 \qquad 0 \leq r \leq \infty \qquad (11)$$

where $\mu = \frac{A_n A_{Fe}}{A_n + A_{Fe}}$ is the reduced mass, A_n and A_{Fe} are the masses of the neutron and the $Fe - 56$, $E_{n,l}$ is the energy, $R_{n,l}(r)$ is the wavefunction and $n = 0, 1, 2, 3, 4$ and $l = 0, 1, 2, 3, 4$ are the energy levels and angular quantum number respectively, r is the distance from the center of the nucleus and $\hbar$ is the reduced Planck's constant.

The term, $\boldsymbol{\frac{l(l+1)}{r^2}}$, is known as the centrifugal potential.

F. Solution to the radial part of the Schrodinger Equation

$$\frac{d^2R_{n,l}(r)}{dr^2} + \frac{2}{r}\frac{dR_{n,l}(r)}{dr} + \frac{2\mu}{\hbar^2}\left(E_{n,l} + V_{mWS}(r) - \frac{\hbar^2 l(l+1)}{2\mu r^2}\right) R_{n,l}(r) = 0 \qquad (12)$$

Let $V_{eff}(r)$ be the effective potential defined by:

$$V_{eff}(r) = V_{mWS}(r) + \frac{l(l+1)}{r^2} = -\frac{V_0}{1+e^{\frac{r-R_0}{a}}} - \frac{W_0 e^{\frac{r-R_0}{a}}}{\left(1+e^{\frac{r-R_0}{a}}\right)^2} + \frac{l(l+1)}{r^2} \qquad (13)$$

Eq. 12 become

$$\frac{d^2R_{n,l}(r)}{dr^2}+\frac{2}{r}\frac{dR_{n,l}(r)}{dr}+\frac{2\mu}{\hbar^2}\left(E_{n,l}-V_{eff}(r)\right)R_{n,l}(r)=0 \quad (14)$$

Using the transformation

$$U_{n,l}(r)=rR_{n,l}(r)$$

$$\Rightarrow R_{n,l}(r)=\frac{U_{n,l}(r)}{r}$$

Differentiating twice, we get

$$\frac{d^2U_{n,l}(r)}{dr^2}=\frac{d^2R_{n,l}(r)}{dr^2}+\frac{2}{r}\frac{dR_{n,l}(r)}{dr} \quad (15)$$

Substituting into Eq. 14, we have

$$\frac{\hbar^2}{2\mu}\left(\frac{d^2U_{n,l}(r)}{dr^2}\right)+\left(E_{n,l}-V_{eff}(r)\right)U_{n,l}(r)=0 \quad (16)$$

Discretizing Eq. 16 using central finite approximation, we get

$$\frac{\hbar^2}{2\mu\hbar^2}\left[\frac{U_{i+1}-2U_i+U_{i-1}}{\Delta r^2}\right]+(E-V_i)U_i=0 \quad (17)$$

where Δr is the step size.

Rearranging,

$$\frac{\hbar^2}{2\mu\Delta r^2}U_{i+1}-\frac{\hbar^2}{2\mu\Delta r^2}(2U_i)+\frac{\hbar^2}{2\mu\Delta r^2}(U_{i-1})+(E-V_iU_i)=0$$

Let $\alpha=\frac{\hbar^2}{2\mu\Delta r^2}$, we have

$$\alpha U_{i-1}+(E-V_i-2\alpha)U_i+\alpha U_{i+1}=0 \quad (18)$$

Boundary Conditions

The wavefunction of the neutron at the left (L) and right (R) sides of the potential (Woods-Saxon potential), in the region $r\in[0,b]$) (fig. 2) is given by:

$$U_L(r)=e^{ik_Lr}+fe^{-ik_Lr} \quad (19a)$$

$$U_R(r)=te^{ik_Rr} \quad (19b)$$

where

$$k_{L,R}=\frac{\sqrt{2\mu(E-V_i)}}{\hbar} \quad (20a)$$

f and t are the amplitudes of the reflected and transmitted waves. At left side of the barrier, the projected neutron is considered as a free particle. Thus,

$$k_L=\frac{\sqrt{2\mu E}}{\hbar} \quad (20b)$$

Applying boundary conditions at mesh 1 where $r=0,-a$

We have from Eq. 19a

$$U_L(0)=U_1=1+f \quad (21a)$$

$$U_L(-a)=U_0=e^{-ik_La}+fe^{ik_La} \quad (21b)$$

At mesh N where $r=b,b+a$

Eq. 19b gives

$$U_R(b)=U_N=te^{ik_Rb} \quad (22a)$$

$$U_R(b+a)=U_{N+1}=te^{ik_R(b+a)} \quad (22b)$$

From Eq. 21a,

$$f = U_1 - 1 \tag{23}$$

Eq. 21b becomes

$$U_0 = e^{-ik_L a} - e^{ik_L a} + e^{ik_L a} U_1$$

$$U_0 = 2isin(k_L a) + e^{ik_L a} U_1 \tag{24}$$

Also, from Eq. 22a

$$t = U_N e^{-ik_R b} \tag{25}$$

And Eq. 22b becomes

$$U_{N+1} = U_N e^{ik_R a} \tag{26}$$

Using Eq. 18, equations at mesh 1 and N can be written as:

At mesh 1

$$\alpha U_0 + (E - V_1 - 2\alpha)U_1 + \alpha U_2 = 0$$

$$\alpha[2isin(k_L a) + U_1] + (E - V_1 - 2\alpha)U_1 + \alpha U_2 = 0$$

$$(E - V_1 - 2\alpha + \alpha e^{ik_L a})U_1 + \alpha U_2 = -2i\alpha sin(k_L a)$$

$$(E - V_1 - 2\alpha + \alpha e^{ik_L a})U_1 + \alpha U_2 = \sigma \tag{27}$$

where

$$\sigma = -2i\alpha sin(k_L a) \tag{28}$$

At mesh N,

$$\alpha U_{N-1} + (E - V_N - 2\alpha)U_N + \alpha U_{N+1} = 0$$

$$\alpha U_{N-1} + (E - V_N - 2\alpha)U_N + \alpha[U_N e^{ik_R a}] = 0$$

$$\alpha U_{N-1} + (E - V_N - 2\alpha + \alpha e^{ik_R a})U_N = 0$$

$$\alpha U_{N-1} + \beta_N U_N = 0 \tag{29}$$

where

$$\beta_N = (E - V_N - 2\alpha + \alpha e^{ik_R a}) \tag{30}$$

Substituting $i = 1, 2, 3, 4, \dots, N-1, N$ successively into Eq. 18, we obtain the following linear system of equations in matrix form:

$$\begin{bmatrix} \beta_1 & \alpha & 0 & 0 & 0 & 0 & . & . \\ \alpha & \beta_2 & \alpha & 0 & 0 & 0 & . & . \\ 0 & \alpha & \beta_3 & \alpha & 0 & 0 & . & . \\ 0 & 0 & \alpha & \beta_4 & \alpha & 0 & . & . \\ . & . & . & . & . & . & . & . \\ . & . & . & . & . & . & . & . \\ . & . & . & . & . & . & . & . \\ . & . & . & . & . & . & \alpha & \beta_N \end{bmatrix} \begin{bmatrix} U_1 \\ U_2 \\ U_3 \\ U_4 \\ . \\ . \\ U_{N-1} \\ U_N \end{bmatrix} = \begin{bmatrix} \sigma \\ 0 \\ 0 \\ 0 \\ . \\ . \\ . \\ 0 \end{bmatrix} \tag{31}$$

$$HU = B \tag{32}$$

where H is an $n \times n$ tridiagonal matrix.

Eq. 32 will give the eigenfunctions of the system of equations with a help of a MATLAB computer code at different energy values of the neutron (guessed values, with an idea of the values from the plot of the Woods-Saxon potential).

G. Probability Current Density

The probability of a neutron to transmit through the Fe-56 after interaction is given by [34] [36]

$$\bar{J} = \frac{i\hbar}{2m}\left[\frac{U\partial U^*}{\partial r} - \frac{U^*\partial U}{\partial r}\right] \tag{33}$$

Incident current density,

$$\bar{J}_{incident} = \frac{i\hbar}{2m}\left[\frac{U_I \partial U_I^*}{\partial r} - \frac{U_I^* \partial U_I}{\partial r}\right]$$

$$\bar{J}_{incident} = \frac{i\hbar}{2m}[(e^{ik_L r}.(-ik_L).e^{-ik_L r}) - (e^{-ik_L r}.(ik_L).e^{ik_L r})]$$

$$\bar{J}_{incident} = \frac{i\hbar}{2m}(-2ik_L) = \hbar k_L \qquad (34)$$

Reflected current density,

$$\bar{J}_{reflected} = \frac{i\hbar}{2m}\left[\frac{U_I \partial U_I^*}{\partial r} - \frac{U_I^* \partial U_I}{\partial r}\right]$$

$$\bar{J}_{reflected} = \frac{i\hbar}{2m}[(fe^{-ik_L r}.(ik_L).fe^{ik_L r}) - (fe^{ik_L r}.(-ik_L).fe^{-ik_L r})]$$

$$\bar{J}_{reflected} = \frac{i\hbar}{2m}(2if^2 k_L) = -f^2\hbar k_L \qquad (35)$$

Transmitted current density,

$$\bar{J}_{transmitted} = \frac{i\hbar}{2m}\left[\frac{U_{III} \partial U_{III}^*}{\partial r} - \frac{U_{III}^* \partial U_{III}}{\partial r}\right]$$

$$\bar{J}_{transmitted} = \frac{i\hbar}{2m}[(te^{ik_R r}.(-ik_R).te^{-ik_R r}) - (te^{-ik_R r}.(ik_R).te^{ik_R r})]$$

$$\bar{J}_{transmitted} = \frac{i\hbar}{2m}(-2it^2 k_R) = t^2\hbar k_R \qquad (36)$$

Transmission coefficient,

$$\tau(E) = \frac{|\bar{J}_{transmitted}|}{|\bar{J}_{incid\,ent}|} = \frac{|t^2|k_R}{k_L} = \frac{|(U_N e^{-ik_R b})^2|k_R}{k_L}$$

$$\tau(E) = \frac{\left|\left(U_N e^{-ik_R b}\right)^2\right|k_R}{k_L} \qquad (37)$$

Reflection coefficient

$$R(E) = 1 - \tau(E)$$

$$R(E) = 1 - \frac{\left|\left(U_N e^{-ik_R b}\right)^2\right|k_R}{k_L} \qquad (38)$$

Eq. 37 and Eq. 38 give the transmission and reflection coefficients of the neutron incident on $Fe-56$ with respect to the energy of the neutron.

III. RESULTS

The results obtained from the simulation are presented below;

A. Wavefunction of the neutron - Fe-56 Interaction for modified Woods-Saxon Potential

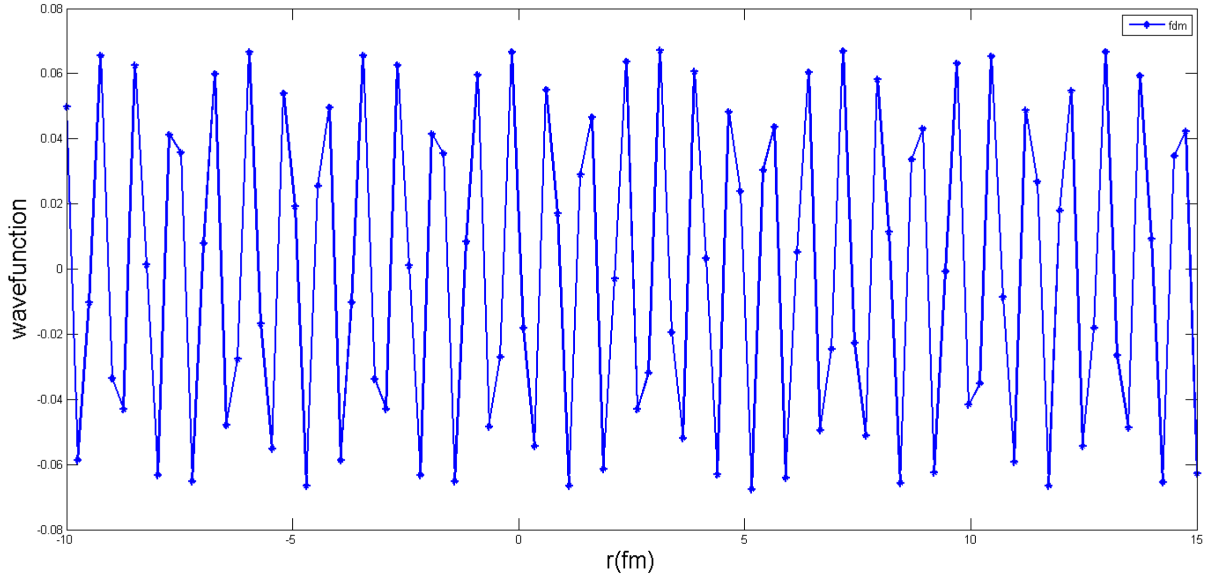

Figure 5: Wave function vs. r(fm) for $W_0 = 50\ MeV, l = 0, a = 0.65\ fm, V_0 = 47.78\ MeV, R_0 = 4.9162\ fm, E = -0.20\ eV$

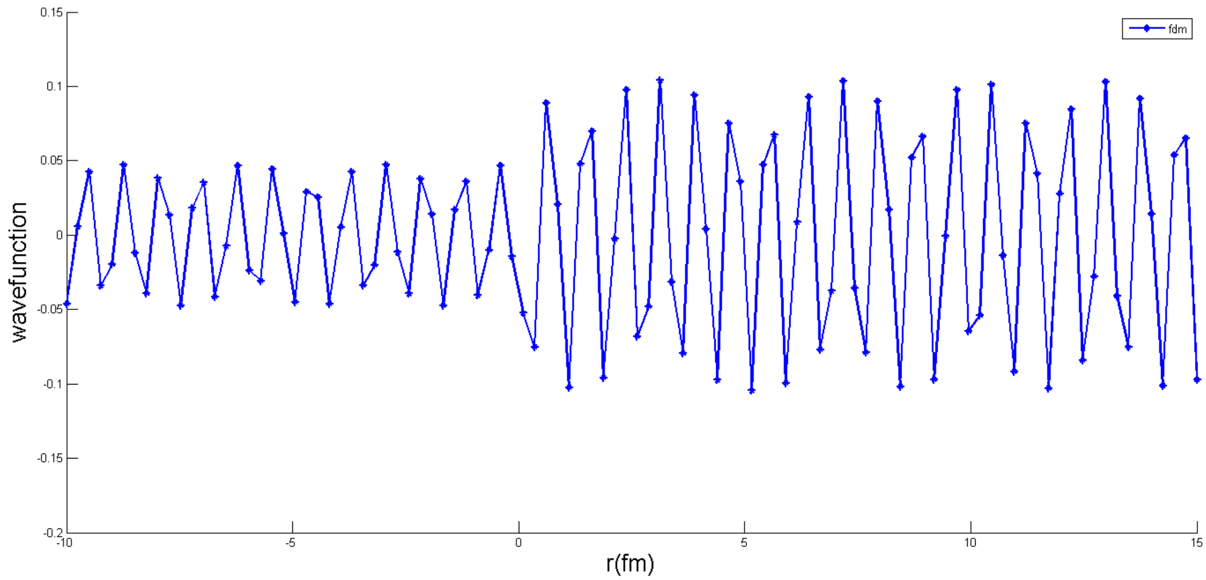

Figure 6: Wave function vs. r(fm) for $W_0 = 50\ MeV, l = 1, a = 0.65 fm, V_0 = 47.78\ MeV, R_0 = 4.9162\ fm, E = -0.20\ eV$

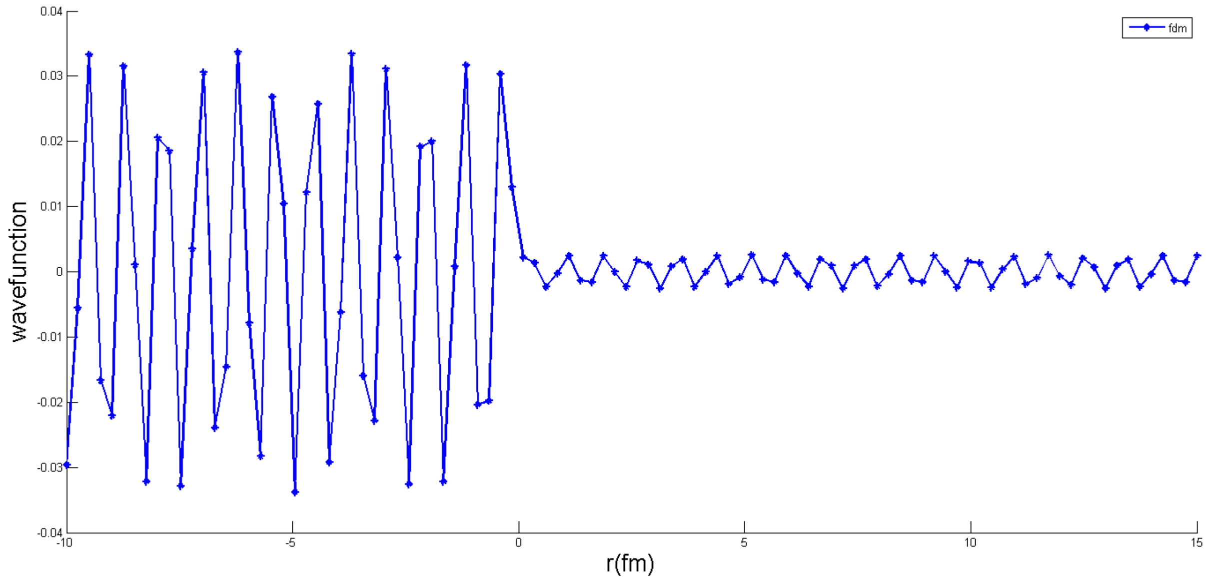

Figure 7: Wave function vs. r(fm) for $W_0 = 50\ MeV, l = 2, a = 0.65\ fm, V_0 = 47.78\ MeV, R_0 = 4.9162\ fm, E = -0.20\ eV$

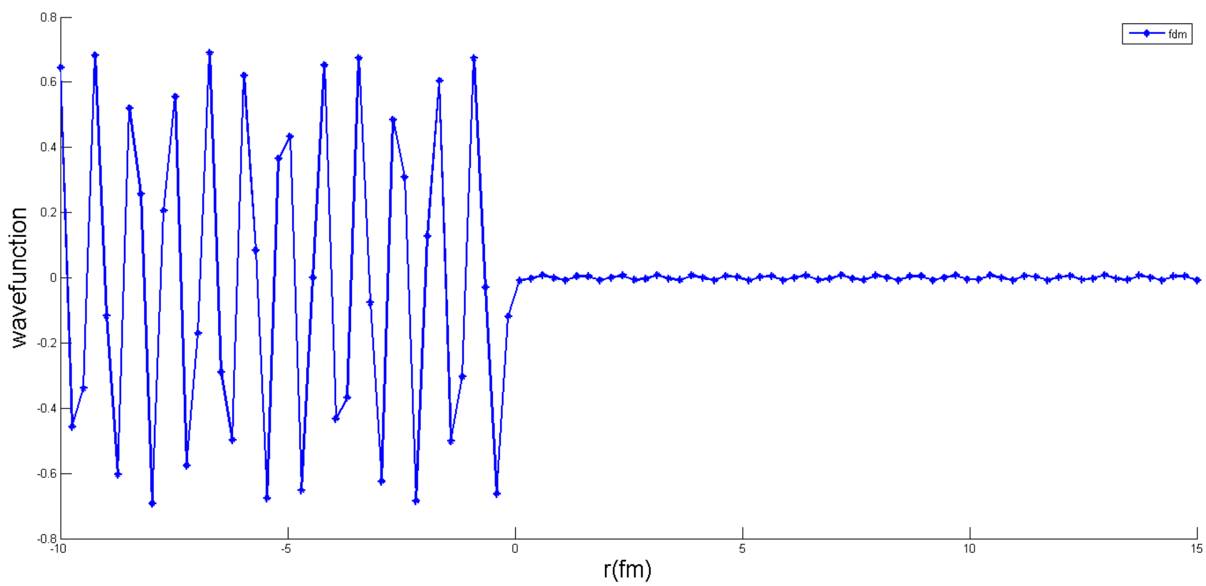

Figure 8: R vs r(fm) for $W_0 = 50\ MeV, l = 3, a = 0.65 fm, V_0 = 47.78\ MeV, R_0 = 4.9162\ fm, E = -0.20\ eV$

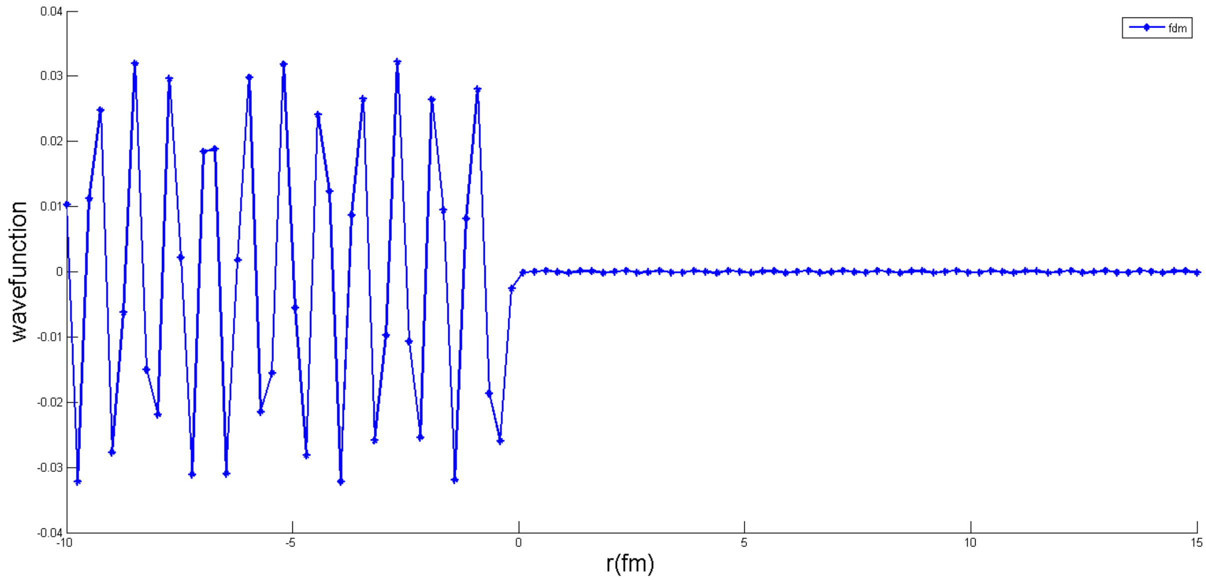

Figure 9: Wave function vs. r(fm) for $W_0 = 50\ MeV, l = 4, a = 0.65\ fm, V_0 = 47.78\ MeV, R_0 = 4.9162\ fm, E = -0.20\ eV$

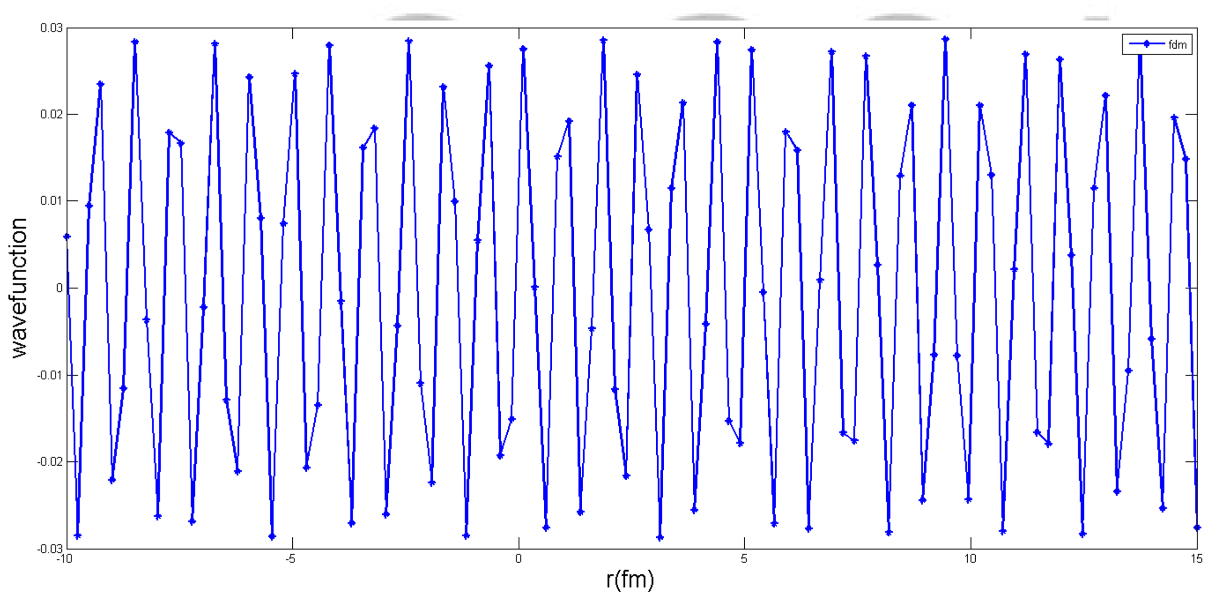

Figure 10: Wave function vs. r(fm) for $W_0 = 50\ MeV, l = 0, a = 0.65\ fm, V_0 = 47.78\ MeV, R_0 = 4.9162\ fm, E = -0.18\ eV$

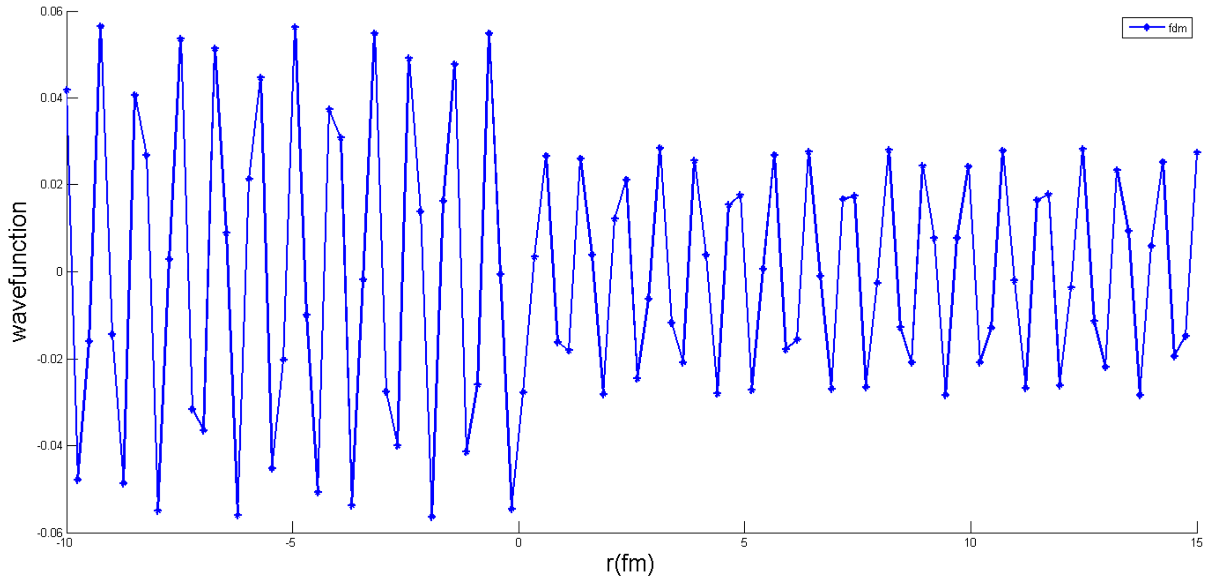

Figure 11: Wave function vs. r(fm) for $W_0 = 50\ MeV, l = 1, a = 0.65\ fm, V_0 = 47.78\ MeV, R_0 = 4.9162\ fm, E = -0.18\ eV$

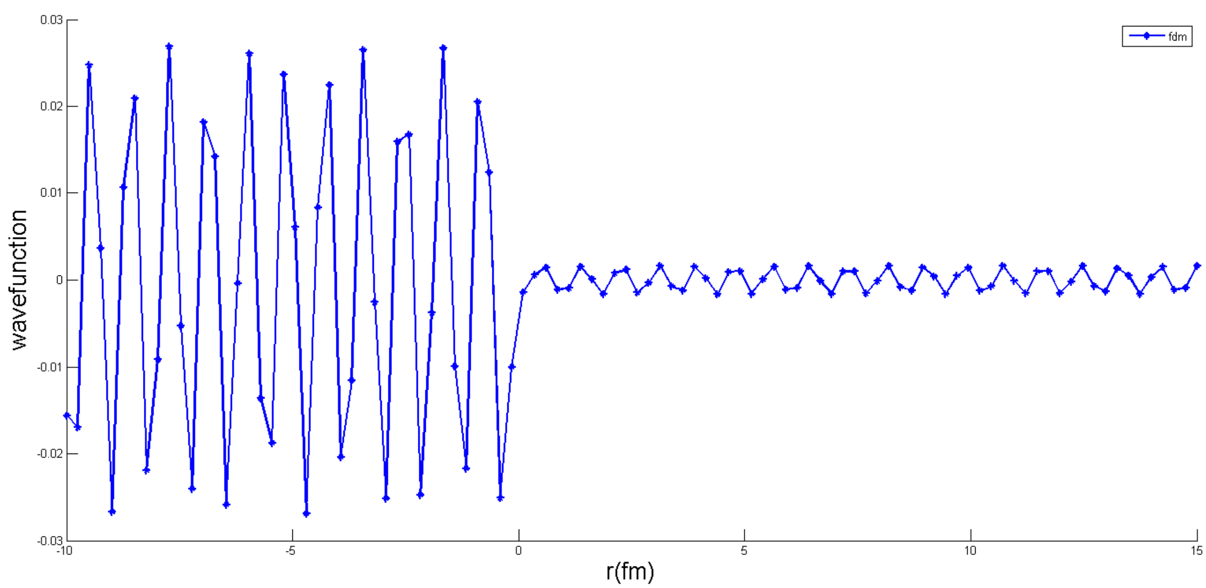

Figure 12: R vs r(fm) for $W_0 = 50\ MeV, l = 2, a = 0.65\ fm, V_0 = 47.78\ MeV, R_0 = 4.9162\ fm, E = -0.18\ eV$

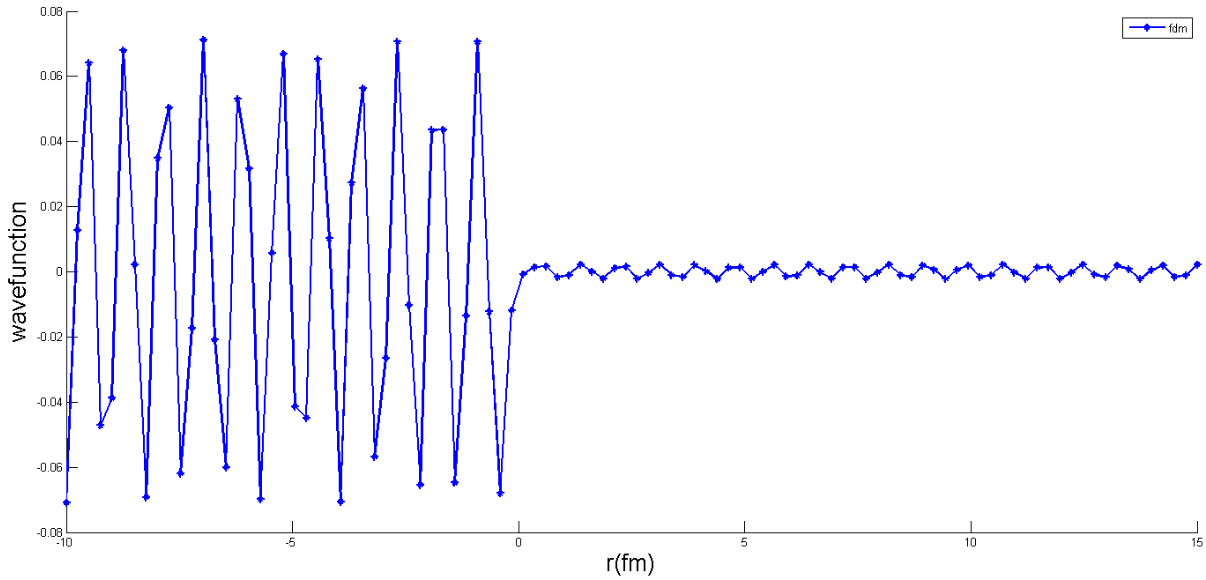

Figure 13: Wave function vs. r(fm) for $W_0 = 50\ MeV, l = 3, a = 0.65\ fm, V_0 = 47.78\ MeV, R_0 = 4.9162\ fm, E = -0.18\ eV$

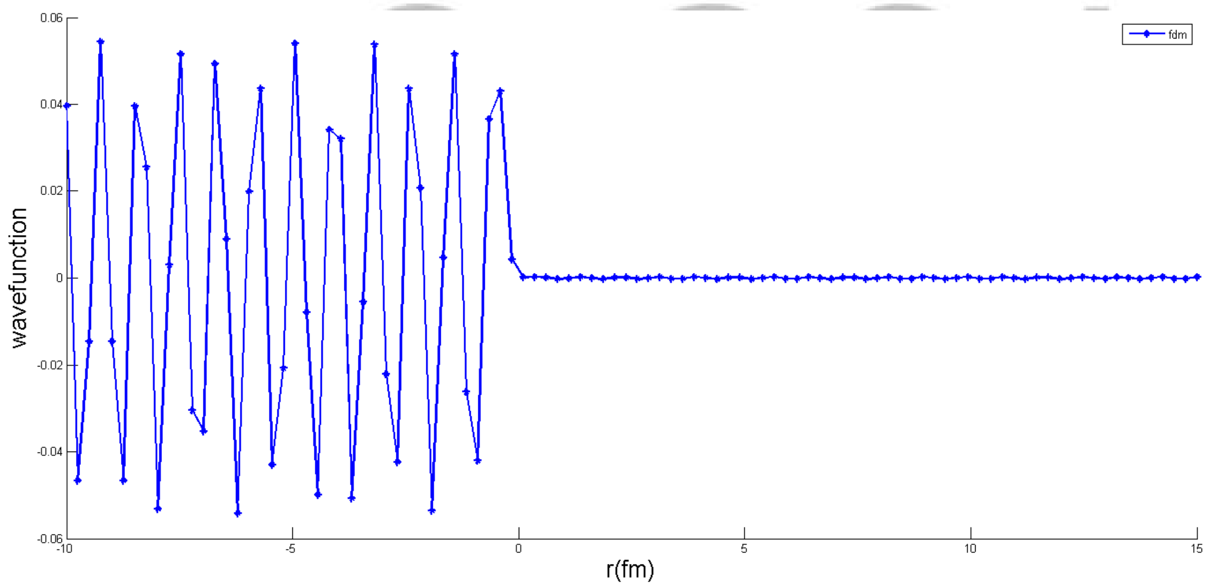

Figure 14: Wave function vs. r(fm) for $W_0 = 50\ MeV, l = 4, a = 0.65\ fm, V_0 = 47.78\ MeV, R_0 = 4.9162\ fm, E = -0.18\ eV$

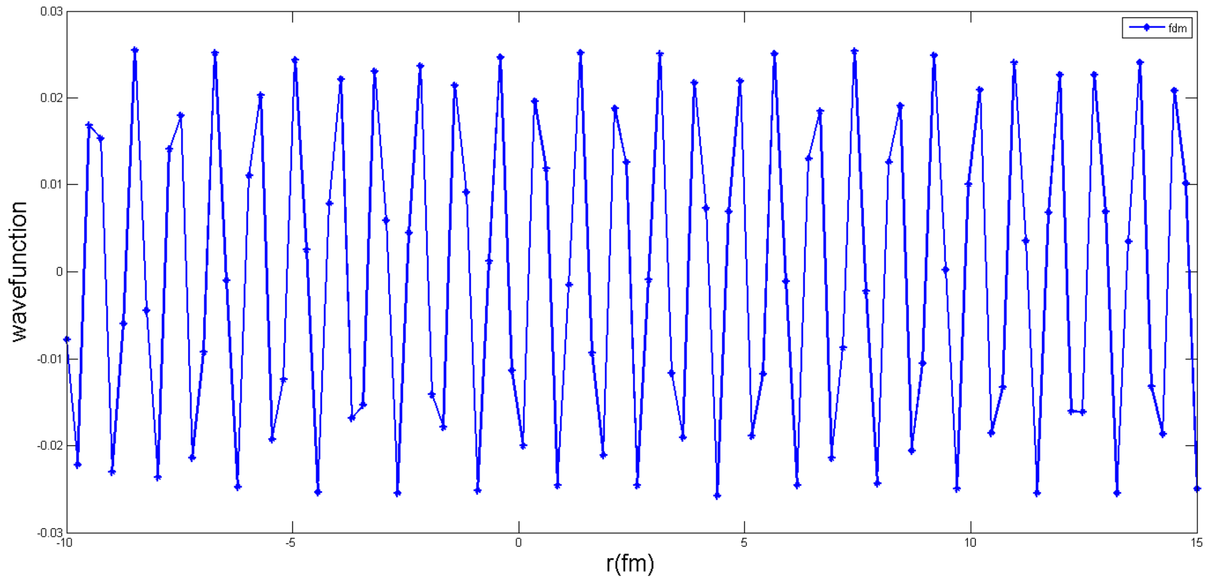

Figure 15: Wave function vs. r(fm) for $W_0 = 50\ MeV, l = 0, a = 0.65\ fm, V_0 = 47.78\ MeV, R_0 = 4.9162\ fm, E = -0.16\ eV$

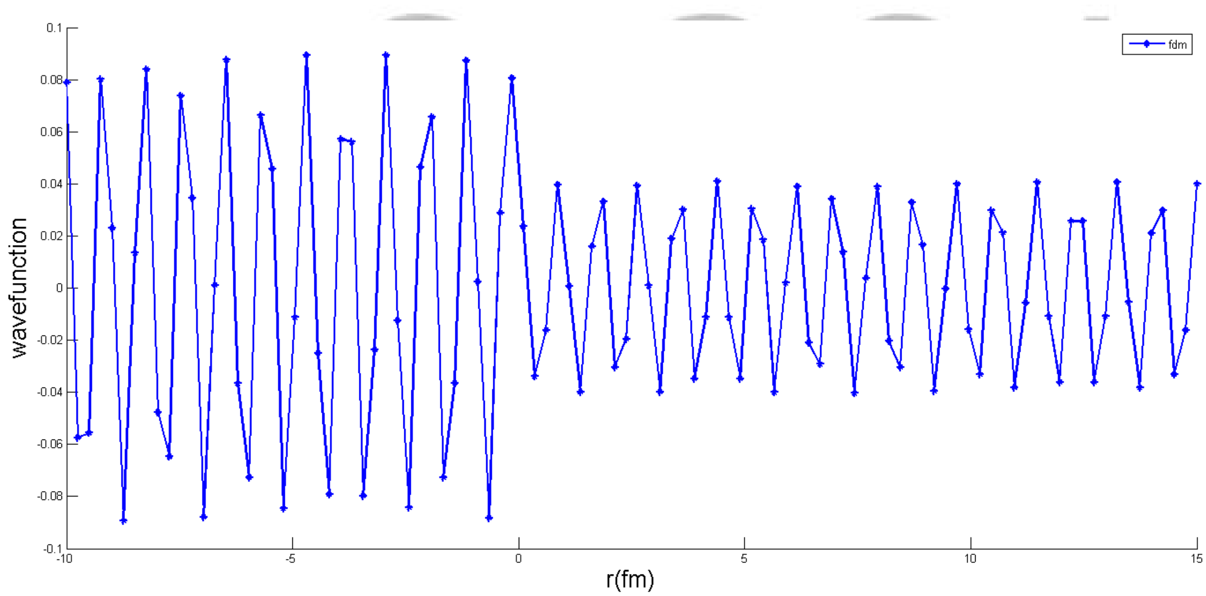

Figure 16: Wave function vs. r(fm) for $W_0 = 50\ MeV, l = 1, a = 0.65\ fm, V_0 = 47.78\ MeV, R_0 = 4.9162\ fm, E = -0.16\ eV$

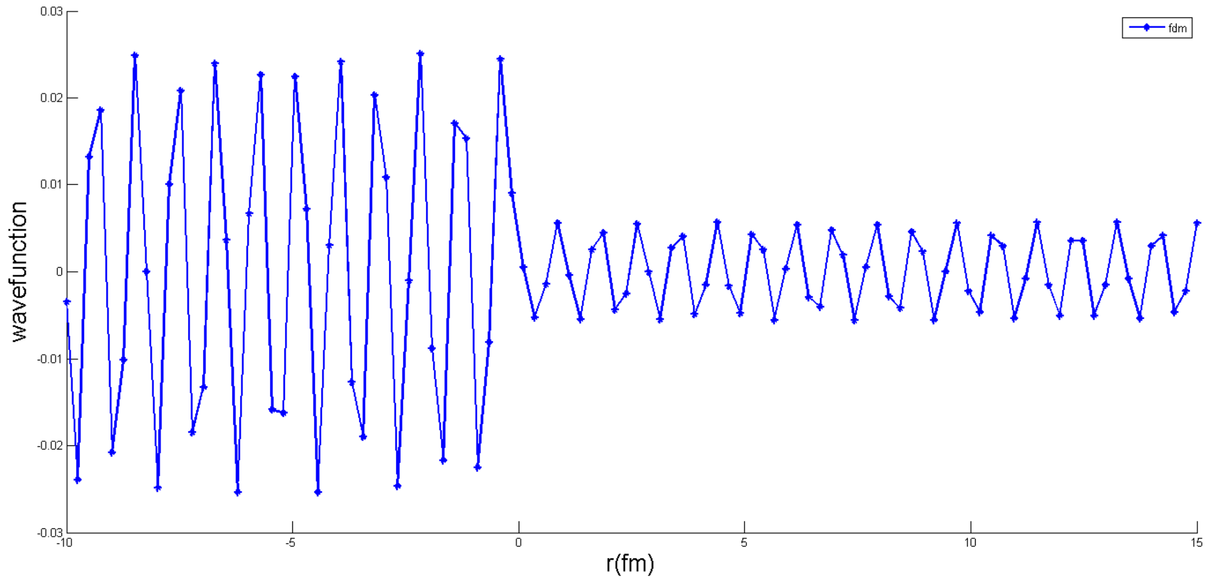

Figure 17: Wave function vs. r(fm) for $W_0 = 50\ MeV, l = 2, a = 0.65\ fm, V_0 = 47.78\ MeV, R_0 = 4.9162\ fm, E = -0.16\ eV$

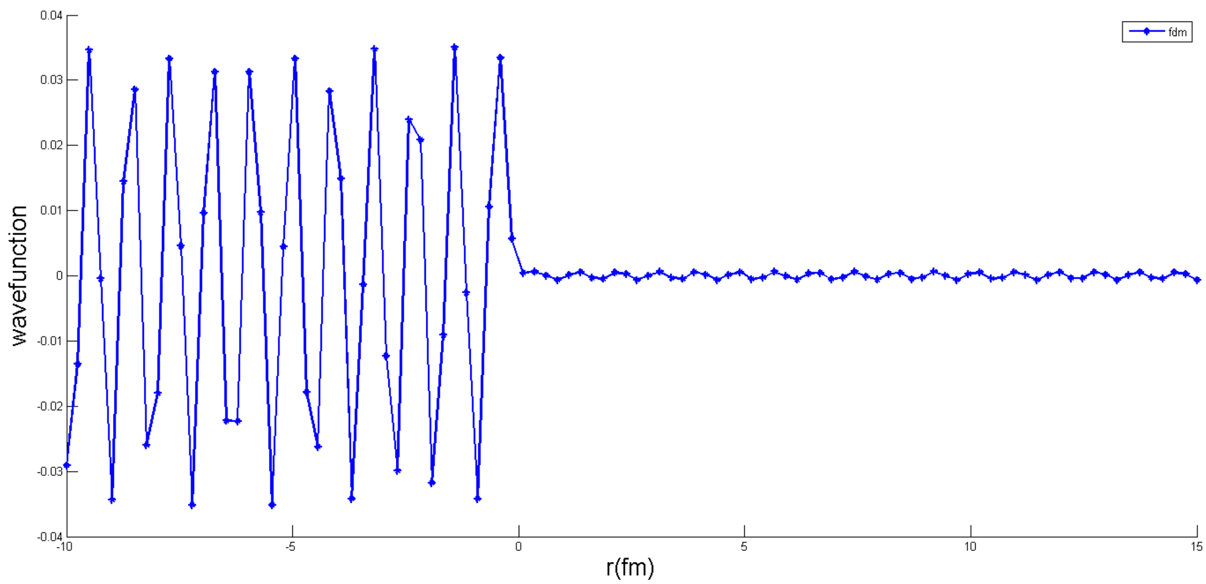

Figure 18: Wave function vs. r(fm) for $W_0 = 50\ MeV, l = 3, a = 0.65\ fm, V_0 = 47.78\ MeV, R_0 = 4.9162\ fm, E = -0.16\ eV$

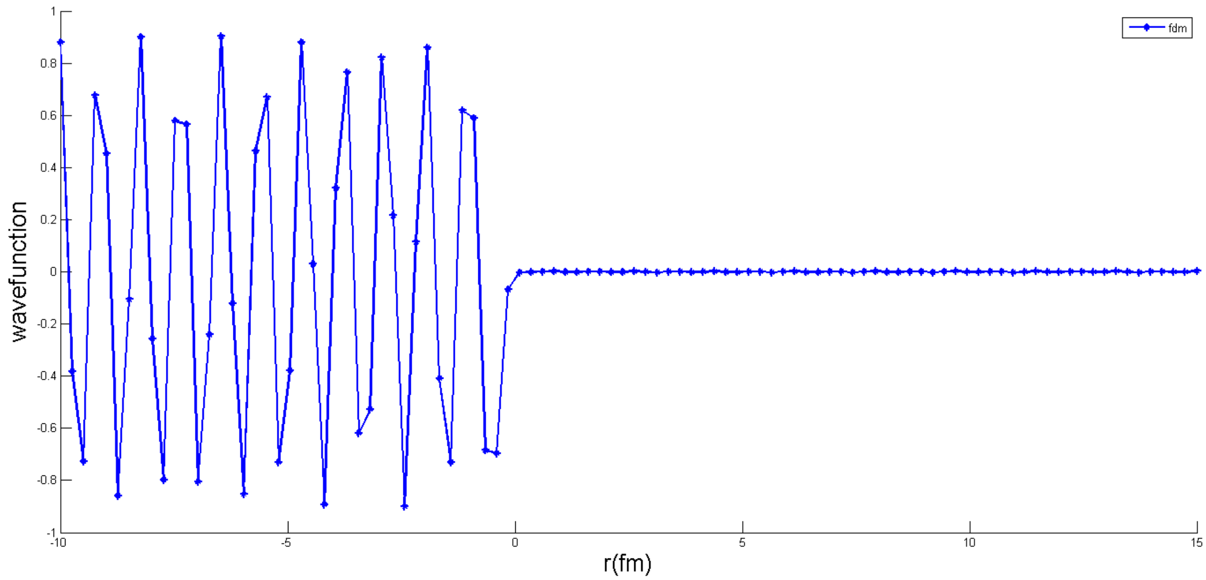

Figure 19: Wave function vs. r(fm) for $W_0 = 50\ MeV, l = 4, a = 0.65\ fm, V_0 = 47.78\ MeV, R_0 = 4.9162\ fm, E = -0.16\ eV$

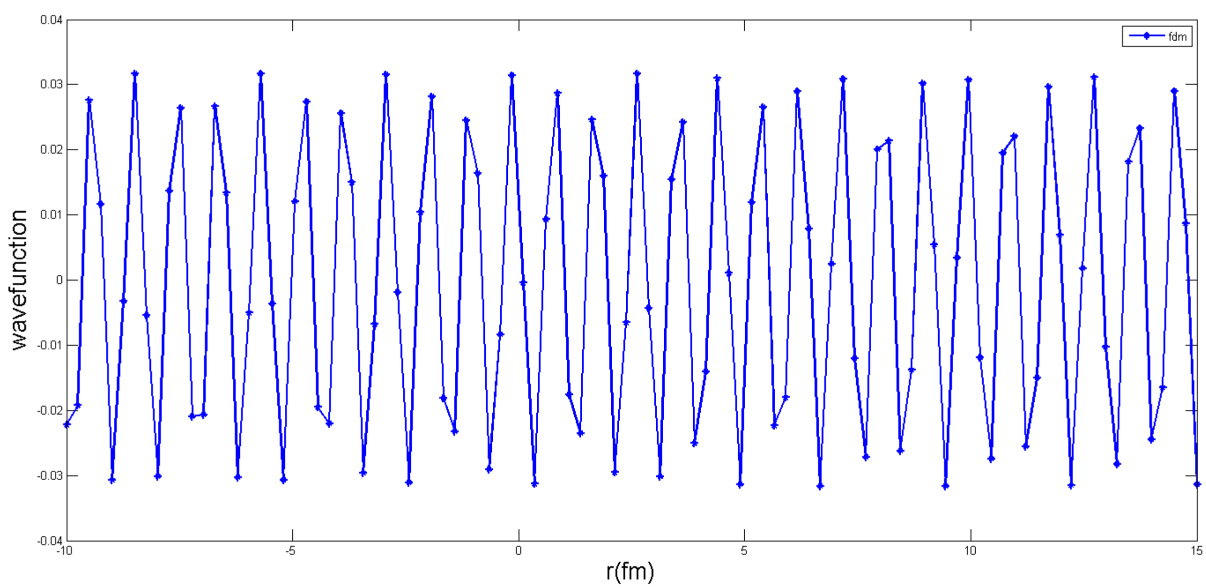

Figure 20: Wave function vs. r(fm) for $W_0 = 50\ MeV, l = 0, a = 0.65\ fm, V_0 = 47.78\ MeV, R_0 = 4.9162\ fm, E = -0.14\ eV$

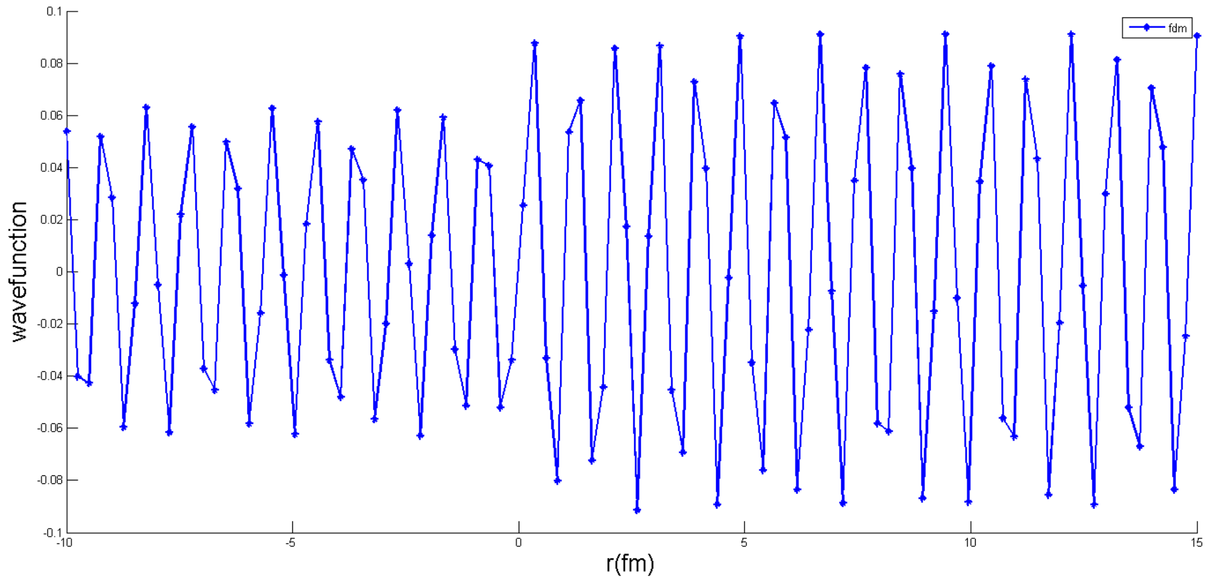

Figure 21: Wave function vs. r(fm) for $W_0 = 50\ MeV, l = 1, a = 0.65\ fm, V_0 = 47.78\ MeV, R_0 = 4.9162\ fm, E = -0.14\ eV$

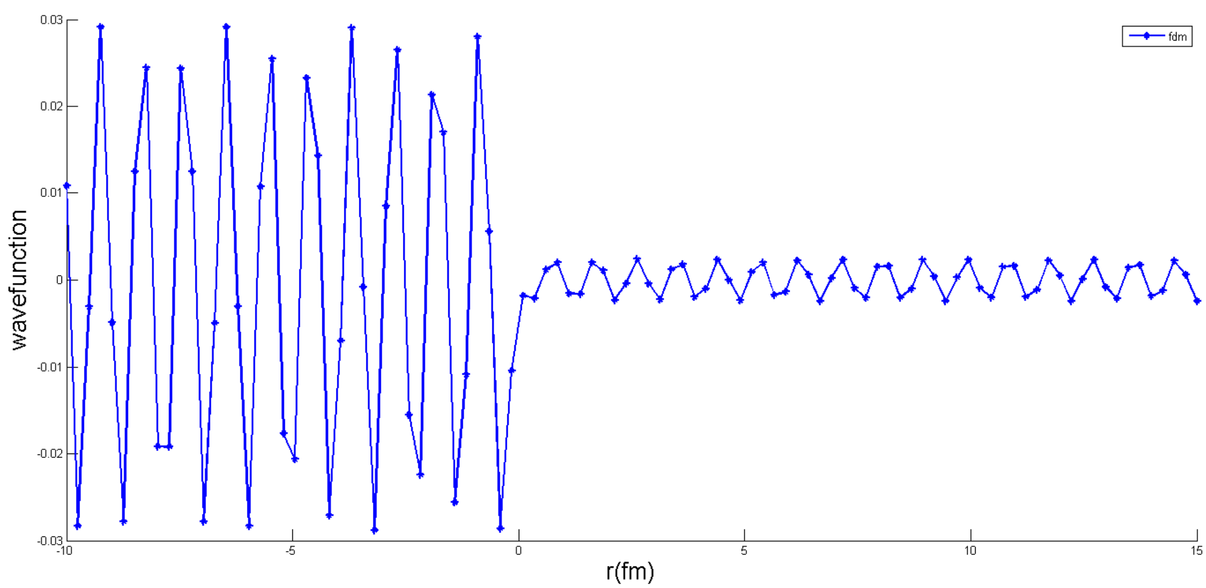

Figure 22: Wave function vs. r(fm) for $W_0 = 50\ MeV, l = 2, a = 0.65\ fm, V_0 = 47.78\ MeV, R_0 = 4.9162\ fm, E = -0.14\ eV$

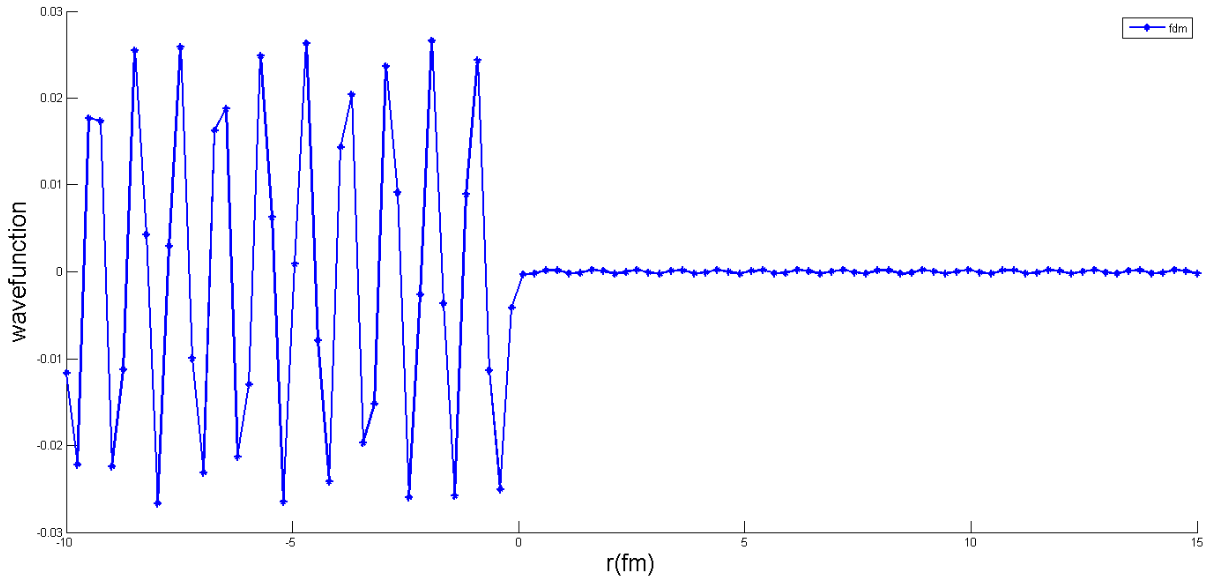

Figure 23: Wave function vs. r(fm) for $W_0 = 50\ MeV, l = 3, a = 0.65\ fm, V_0 = 47.78\ MeV, R_0 = 4.9162\ fm, E = -0.14\ eV$

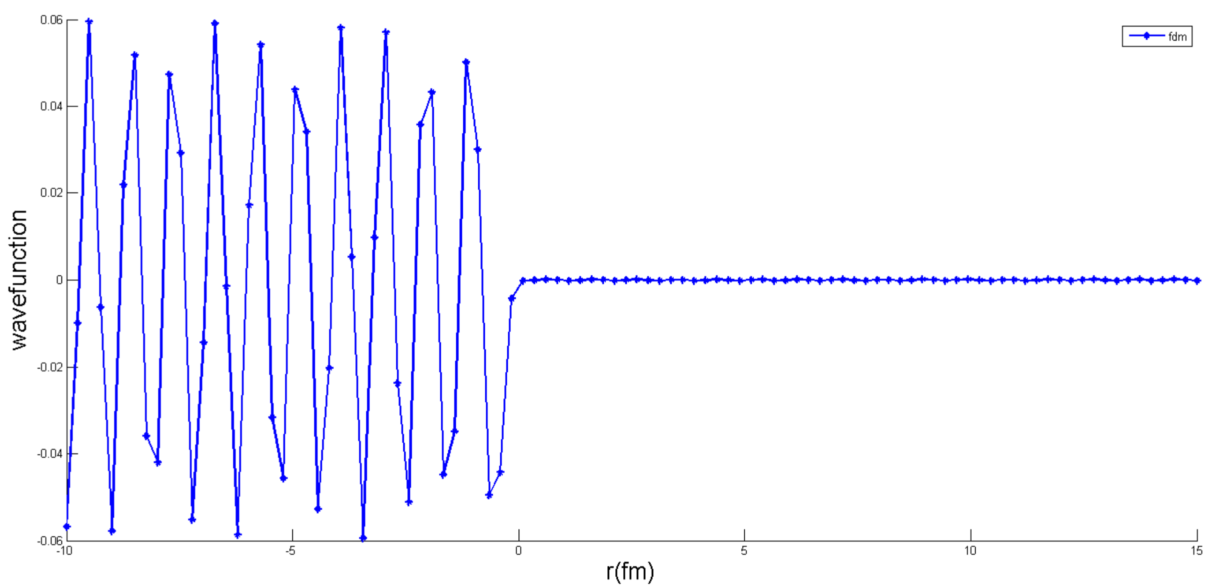

Figure 24: Wave function vs. r(fm) for $W_0 = 50\ MeV, l = 4, a = 0.65\ fm, V_0 = 47.78\ MeV, R_0 = 4.9162\ fm, E = -0.14\ eV$

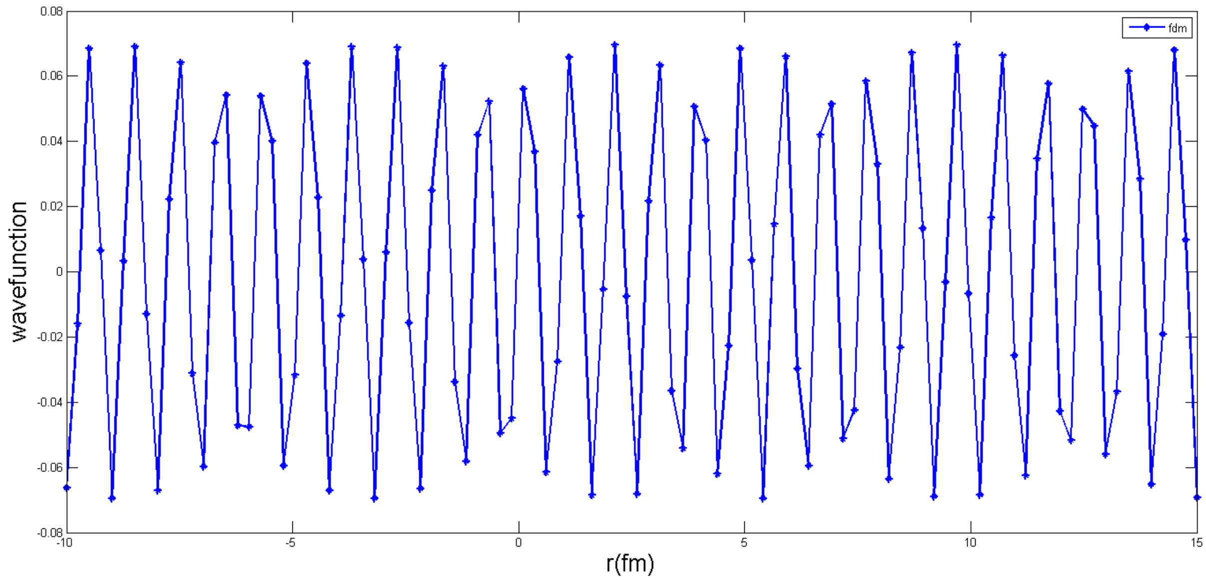

Figure 25: Wave function vs. r(fm) for $W_0 = 50\ MeV, l = 0, a = 0.65\ fm, V_0 = 47.78\ MeV, R_0 = 4.9162\ fm, E = -0.12\ eV$

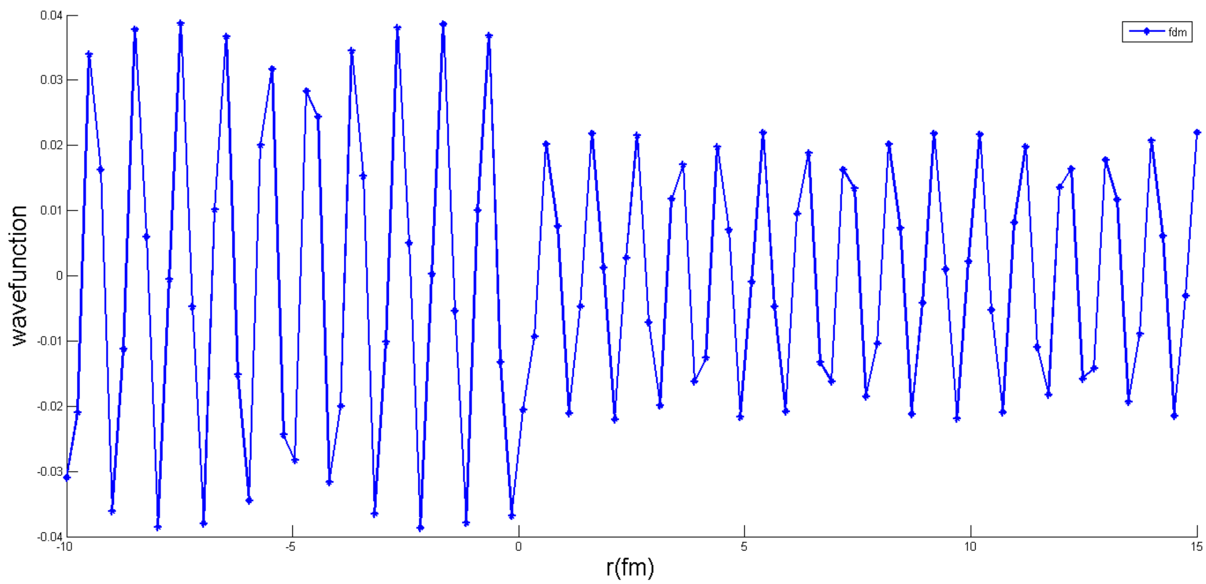

Figure 26: Wave function vs. r(fm) for $W_0 = 50\ MeV, l = 1, a = 0.65\ fm, V_0 = 47.78\ MeV, R_0 = 4.9162\ fm, E = -0.12\ eV$

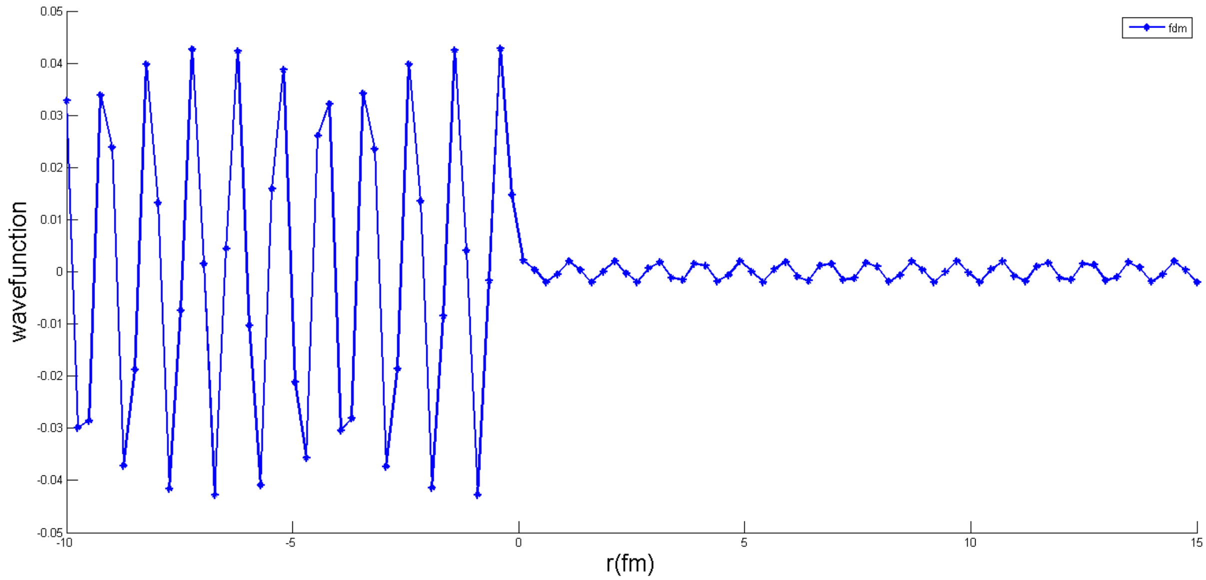

Figure 27: Wave function vs. r(fm) for $W_0 = 50\ MeV, l = 2, a = 0.65\ fm, V_0 = 47.78\ MeV, R_0 = 4.9162\ fm, E = -0.12\ eV$

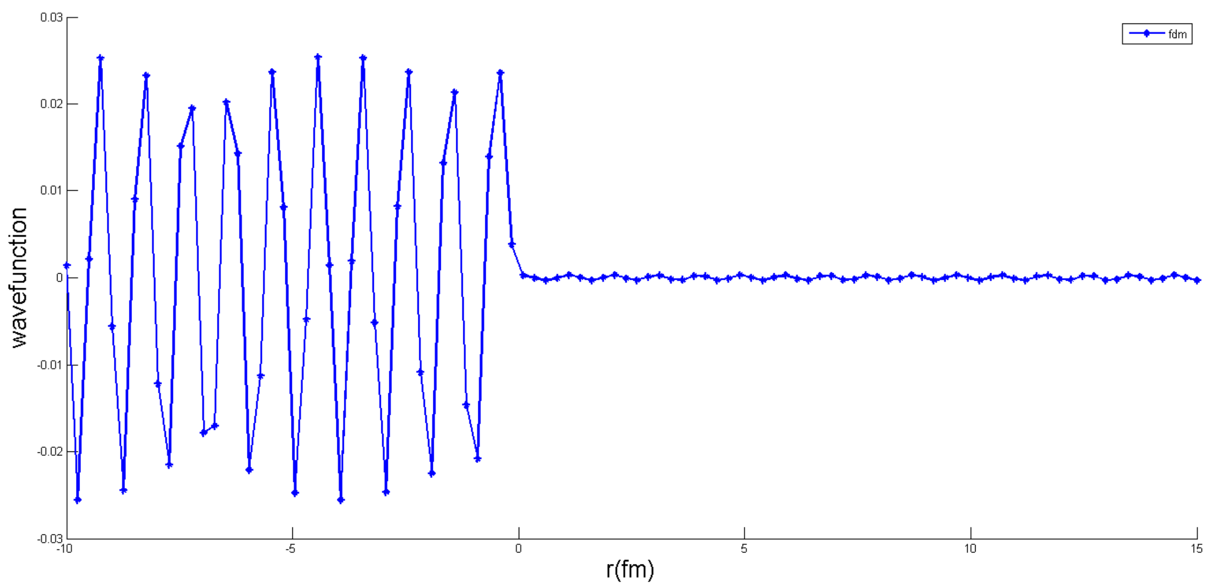

Figure 28: Wave function vs. r(fm) for $W_0 = 50\ MeV, l = 3, a = 0.65\ fm, V_0 = 47.78\ MeV, R_0 = 4.9162\ fm, E = -0.12\ eV$

GSJ: Volume 10, Issue 5, May 2022
ISSN 2320-9186

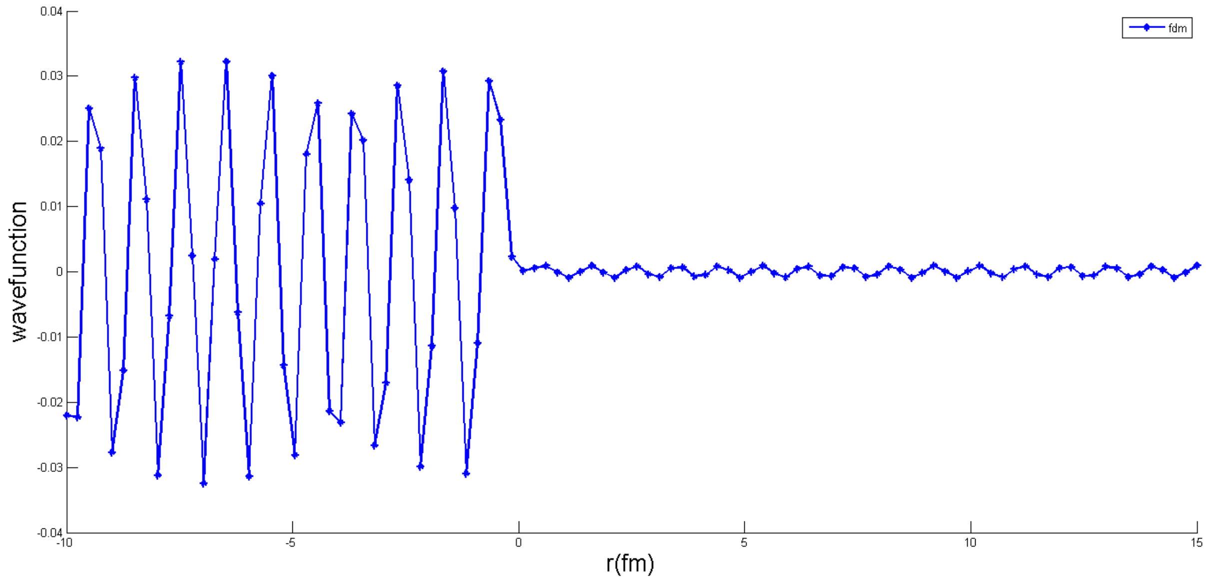

Figure 29: Wave function vs. r(fm) for $W_0 = 50\ MeV, l = 4, a = 0.65\ fm, V_0 = 47.78\ MeV, R_0 = 4.9162\ fm, E = -0.12\ eV$

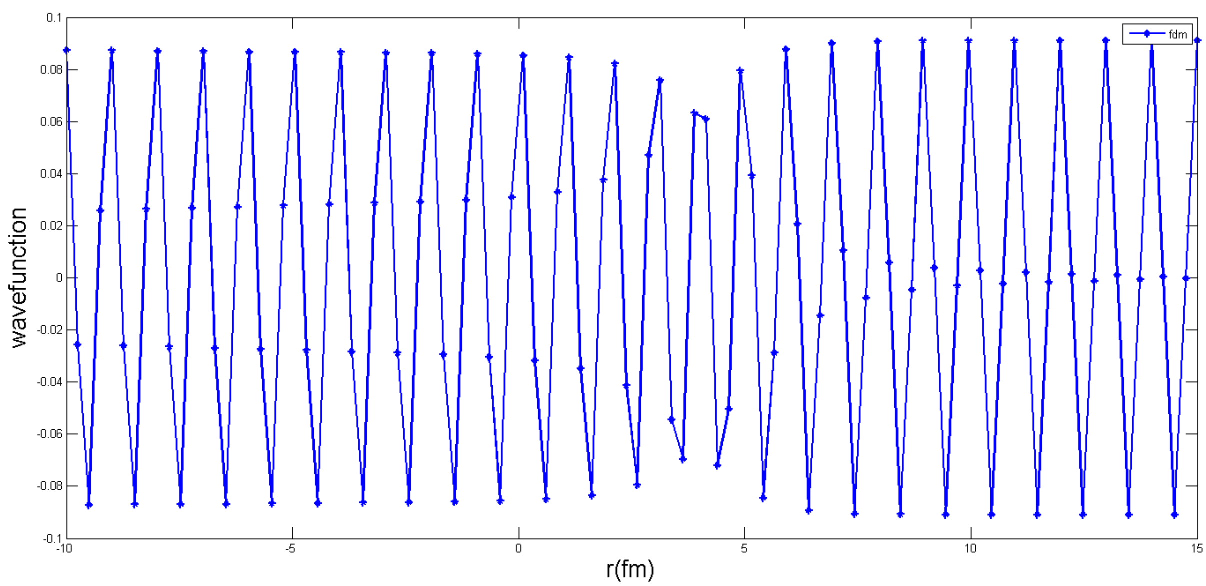

Figure 30: Wave function vs. r(fm) for $W_0 = 50\ MeV, l = 0, a = 0.65\ fm, V_0 = 47.78\ MeV, R_0 = 4.9162\ fm, E = -0.10\ eV$

GSJ: Volume 10, Issue 5, May 2022
ISSN 2320-9186

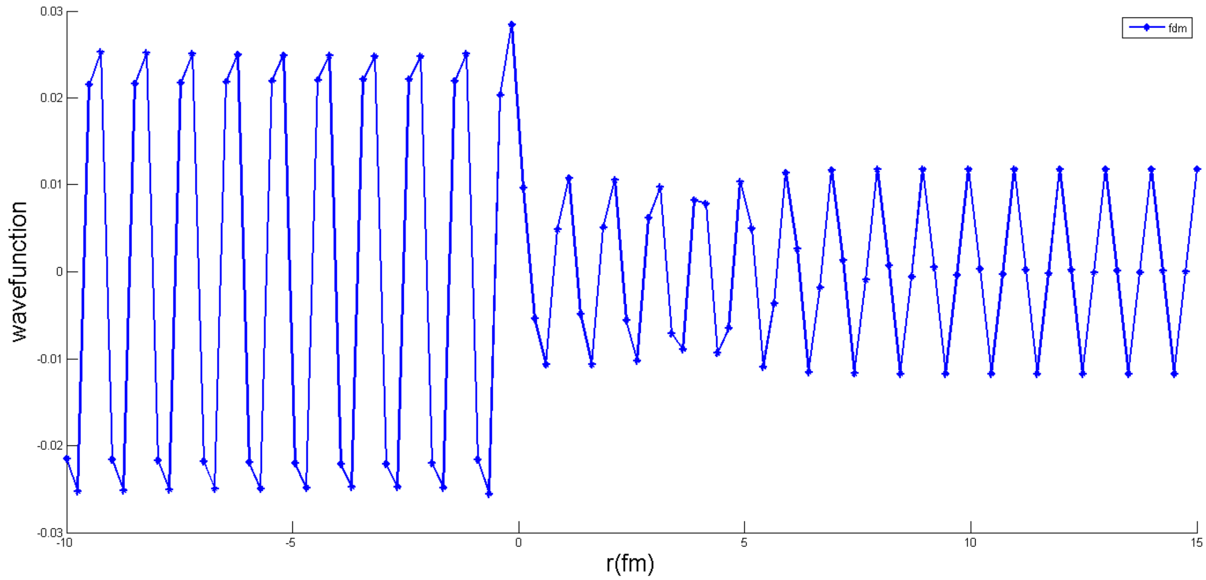

Figure 31: Wave function vs. r(fm) for $W_0 = 50\ MeV, l = 1, a = 0.65\ fm, V_0 = 47.78\ MeV, R_0 = 4.9162\ fm, E = -0.10\ eV$

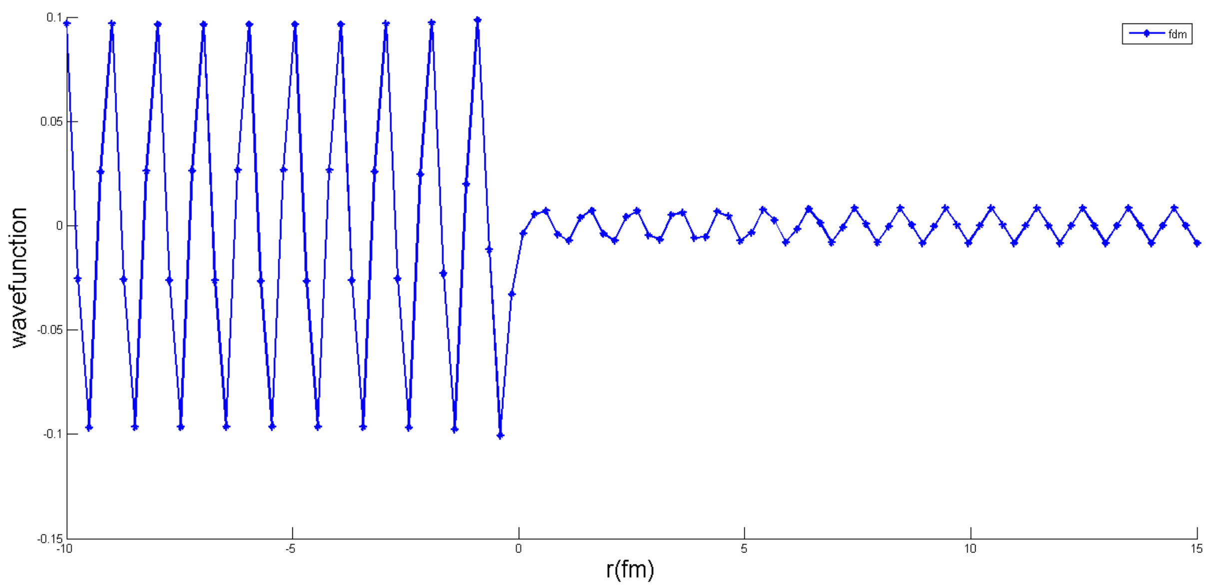

Figure 32: Wave function vs. r(fm) for $W_0 = 50\ MeV, l = 2, a = 0.65\ fm, V_0 = 47.78\ MeV, R_0 = 4.9162\ fm, E = -0.10\ eV$

GSJ: Volume 10, Issue 5, May 2022
ISSN 2320-9186

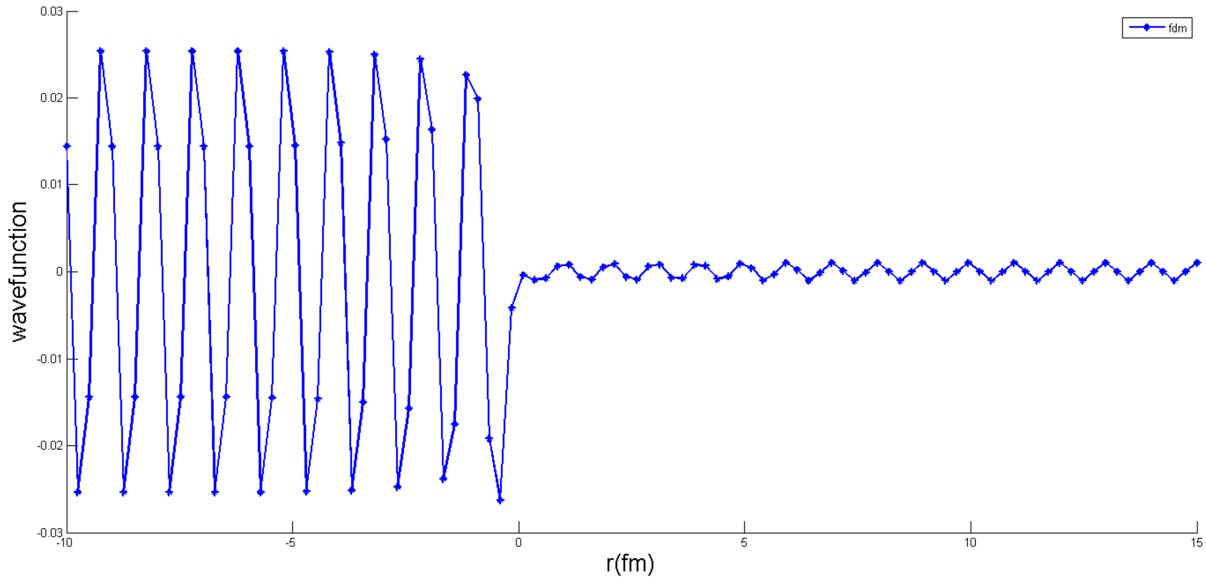

Figure 33: Wave function vs. r(fm) for $W_0 = 50\ MeV, l = 3, a = 0.65\ fm, V_0 = 47.78\ MeV, R_0 = 4.9162\ fm, E = -0.10\ eV$

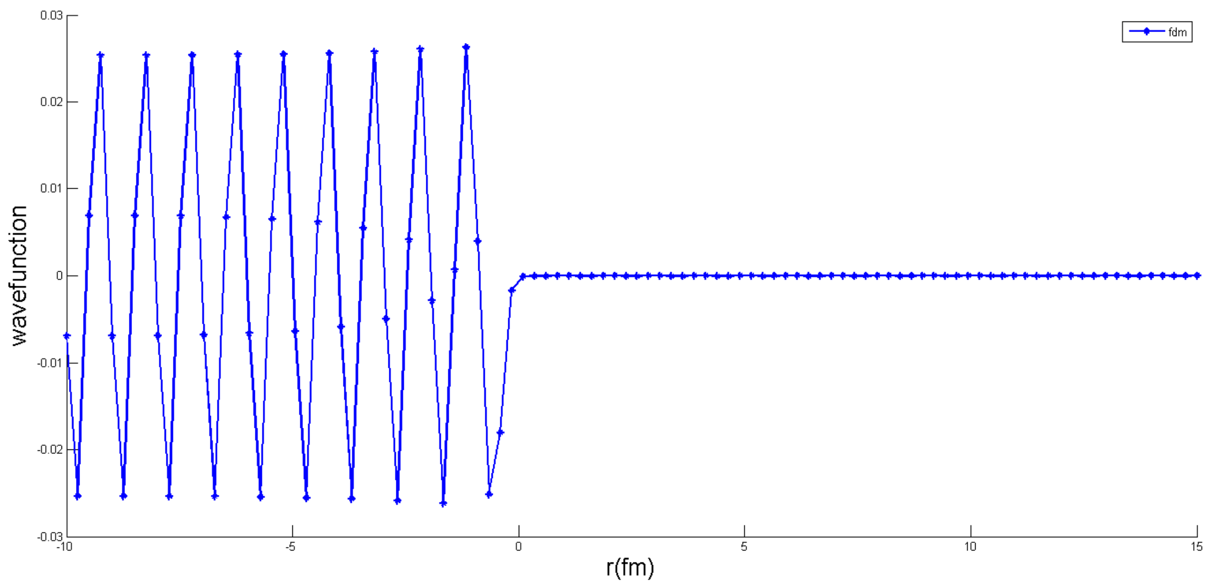

Figure 34: Wave function vs. r(fm) for $W_0 = 50\ MeV, l = 4, a = 0.65\ fm, V_0 = 47.78\ MeV, R_0 = 4.9162\ fm, E = -0.10\ eV$

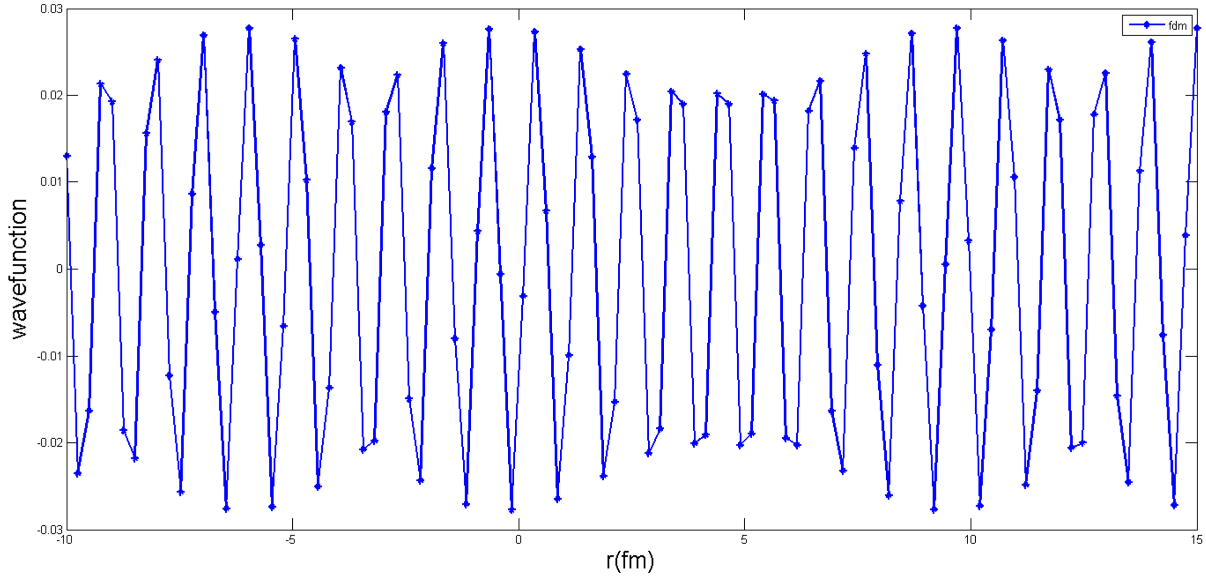

Figure 35: Wave function vs. r(fm) for $W_0 = 50\ MeV, l = 0, a = 0.65\ fm, V_0 = 47.78\ MeV, R_0 = 4.9162\ fm, E = -0.08\ eV$

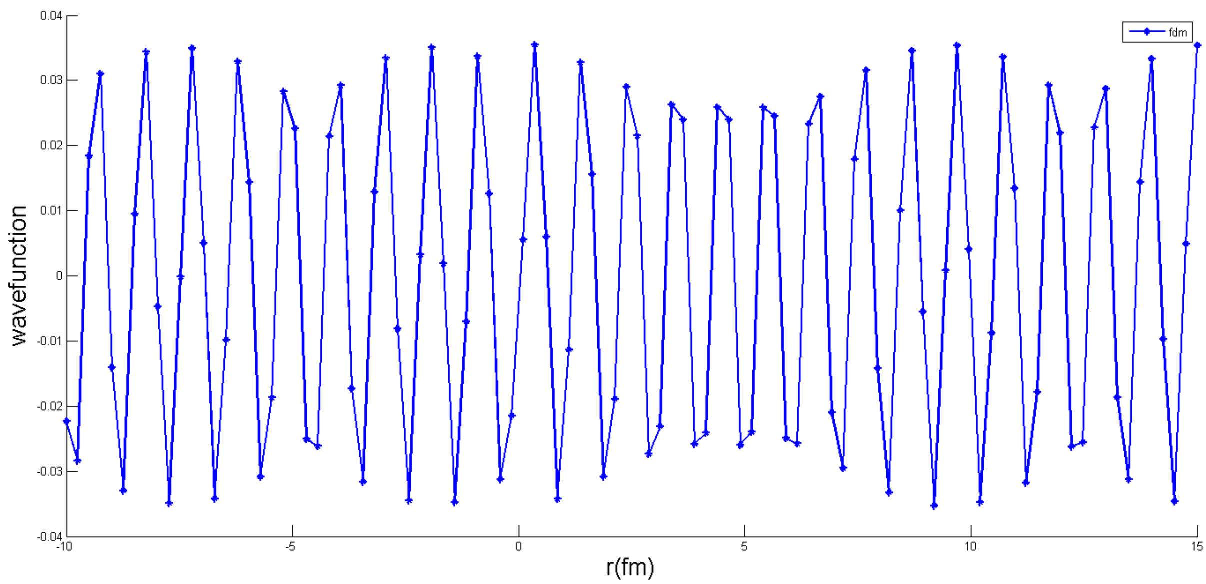

Figure 36: Wave function vs. r(fm) for $W_0 = 50\ MeV, l = 1, a = 0.65\ fm, V_0 = 47.78\ MeV, R_0 = 4.9162\ fm, E = -0.08\ eV$

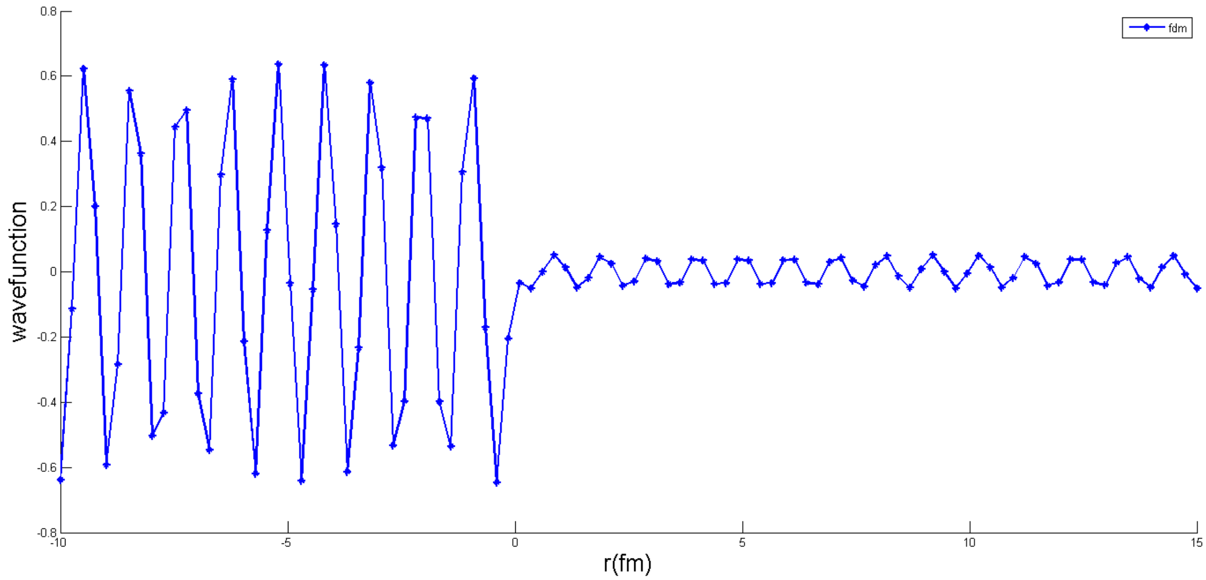

Figure 37: Wave function vs. r(fm) for $W_0 = 50\ MeV, l = 2, a = 0.65\ fm, V_0 = 47.78\ MeV, R_0 = 4.9162\ fm, E = -0.08\ eV$

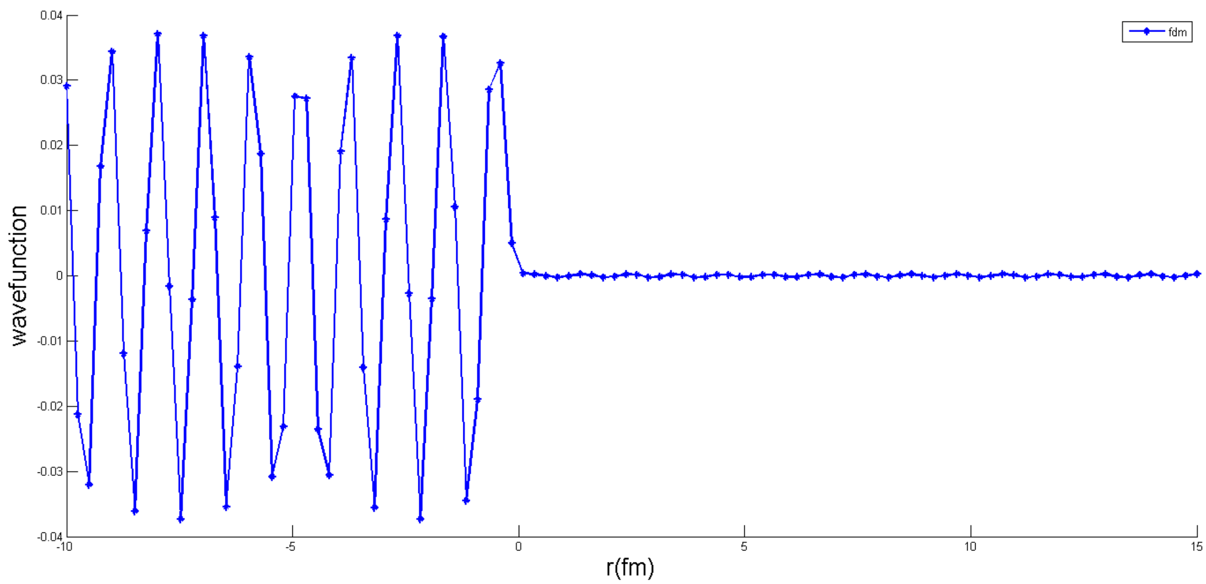

Figure 38: Wave function vs. r(fm) for $W_0 = 50\ MeV, l = 3, a = 0.65\ fm, V_0 = 47.78\ MeV, R_0 = 4.9162\ fm, E = -0.08\ eV$

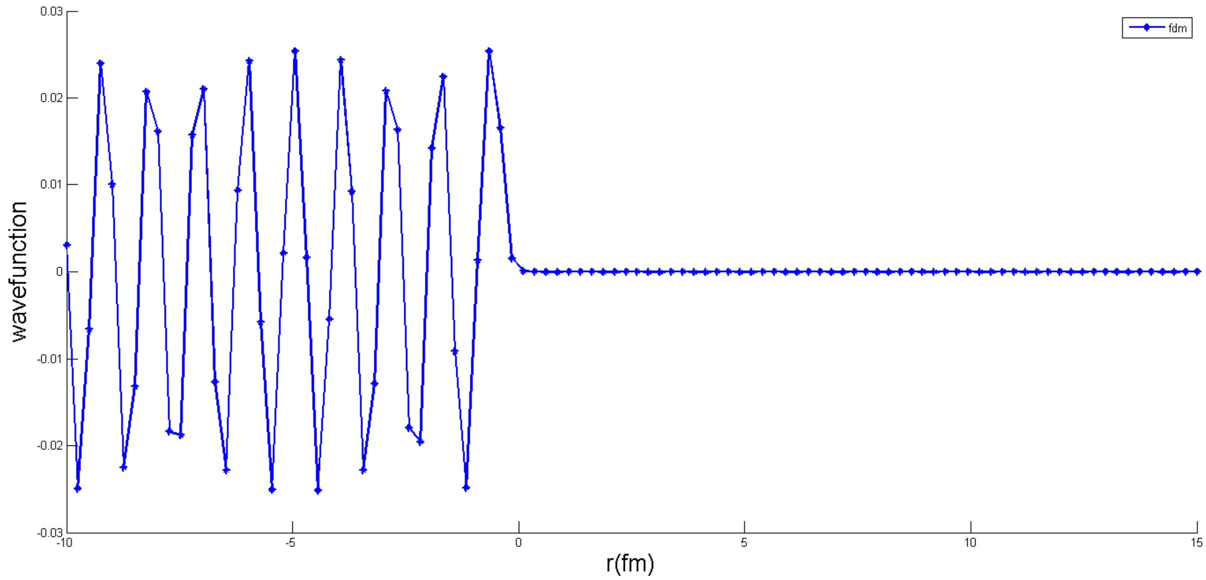

Figure 39: Wave function vs. r(fm) for $W_0 = 50\ MeV, l = 4, a = 0.65\ fm, V_0 = 47.78\ MeV, R_0 = 4.9162\ fm, E = -0.08\ eV$

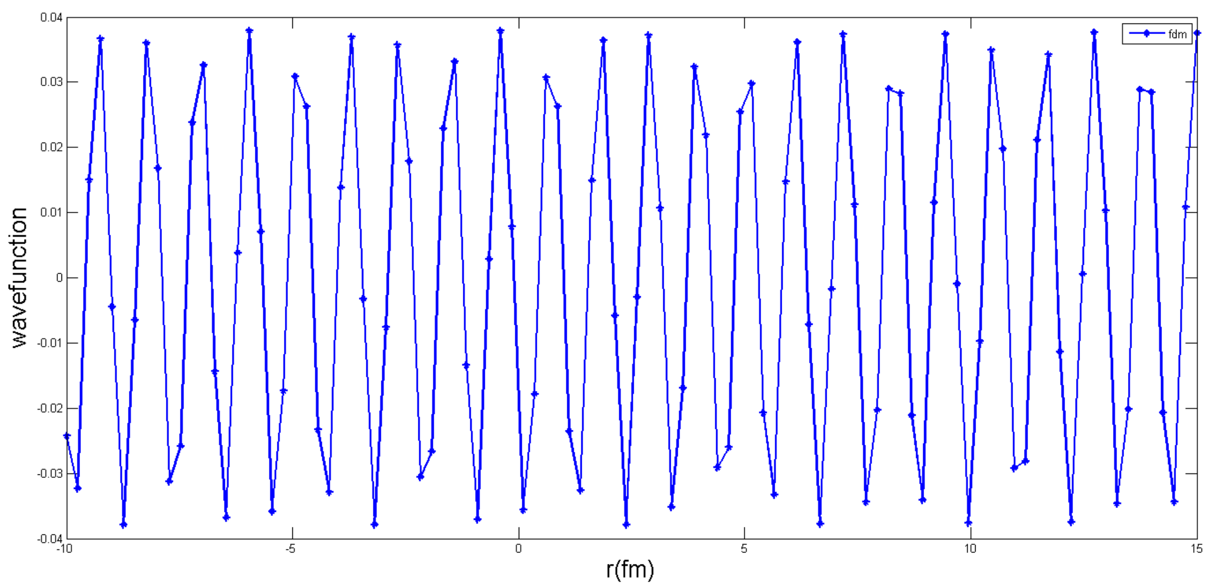

Figure 40: Wave function vs. r(fm) for $W_0 = 50\ MeV, l = 0, a = 0.65\ fm, V_0 = 47.78\ MeV, R_0 = 4.9162\ fm, E = -0.06\ eV$

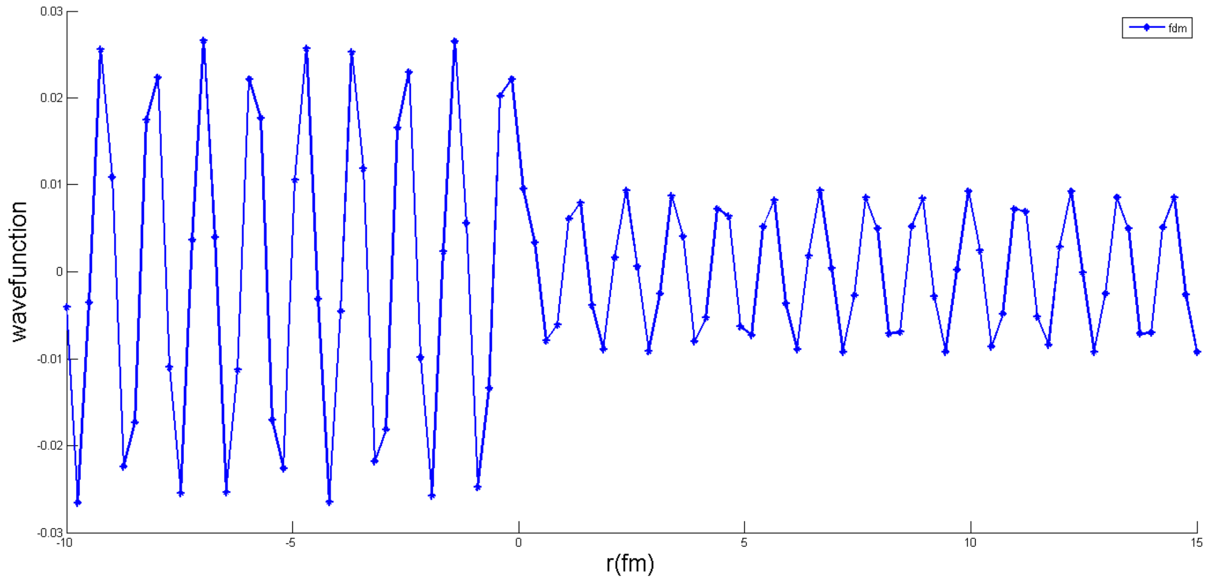

Figure 41: Wave function vs. r(fm) for $W_0 = 50\ MeV, l = 1, a = 0.65\ fm, V_0 = 47.78\ MeV, R_0 = 4.9162\ fm, E = -0.06\ eV$

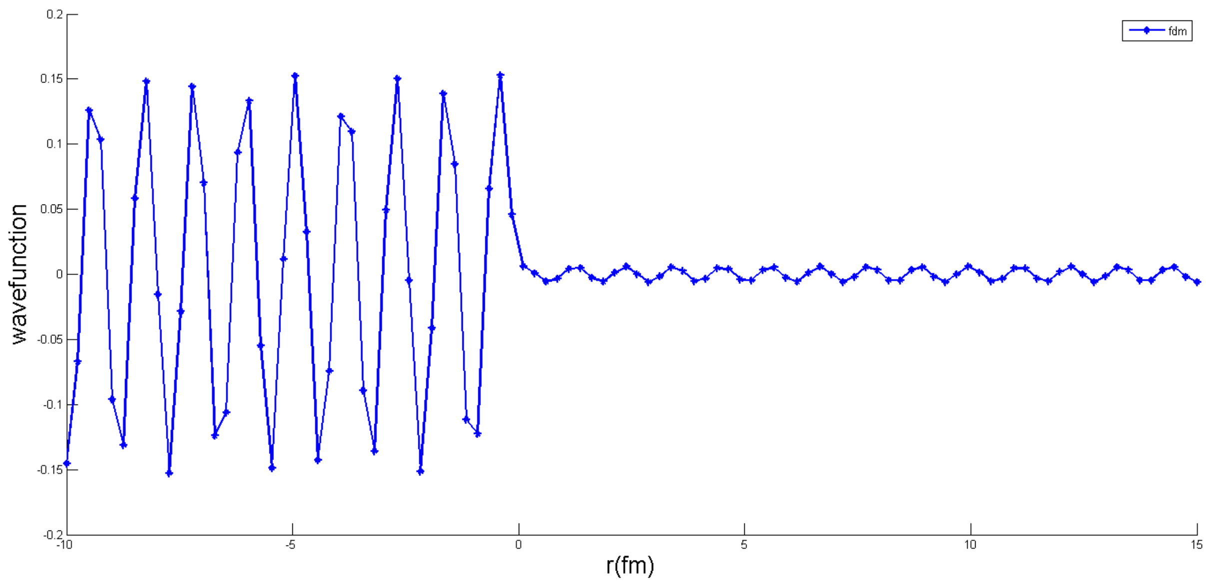

Figure 42: Wave function vs. r(fm) for $W_0 = 50\ MeV, l = 2, a = 0.65\ fm, V_0 = 47.78\ MeV, R_0 = 4.9162\ fm, E = -0.06\ eV$

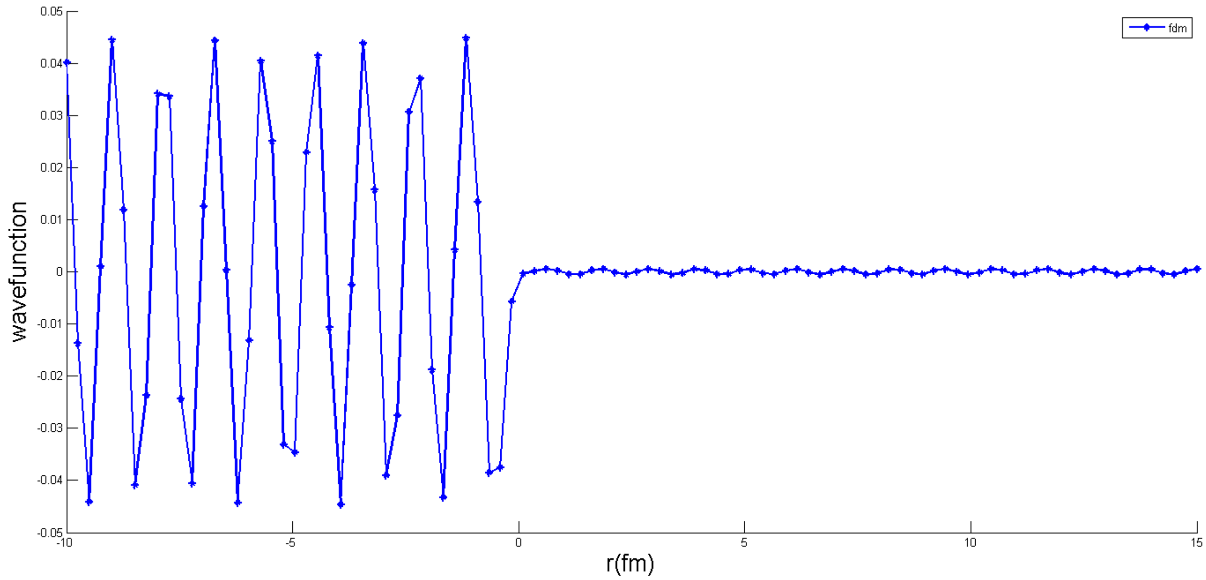

Figure 43: Wave function vs. r(fm) for $W_0 = 50\ MeV, l = 3, a = 0.65\ fm, V_0 = 47.78\ MeV, R_0 = 4.9162\ fm, E = -0.06\ eV$

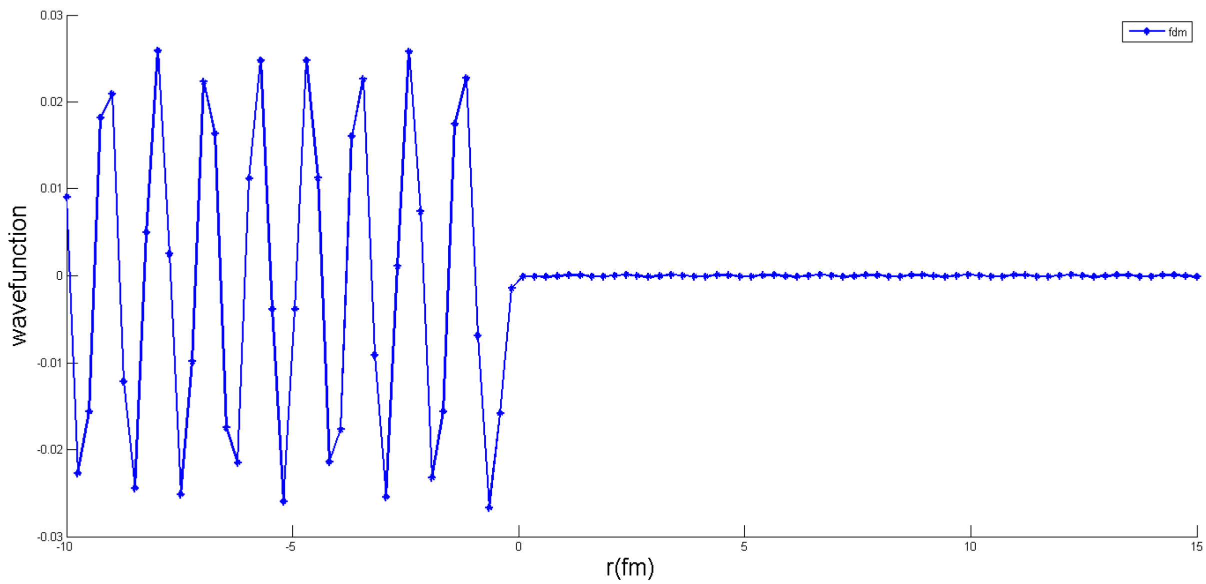

Figure 44: Wave function vs. r(fm) for $W_0 = 50\ MeV, l = 4, a = 0.65\ fm, V_0 = 47.78\ MeV, R_0 = 4.9162\ fm, E = -0.06\ eV$

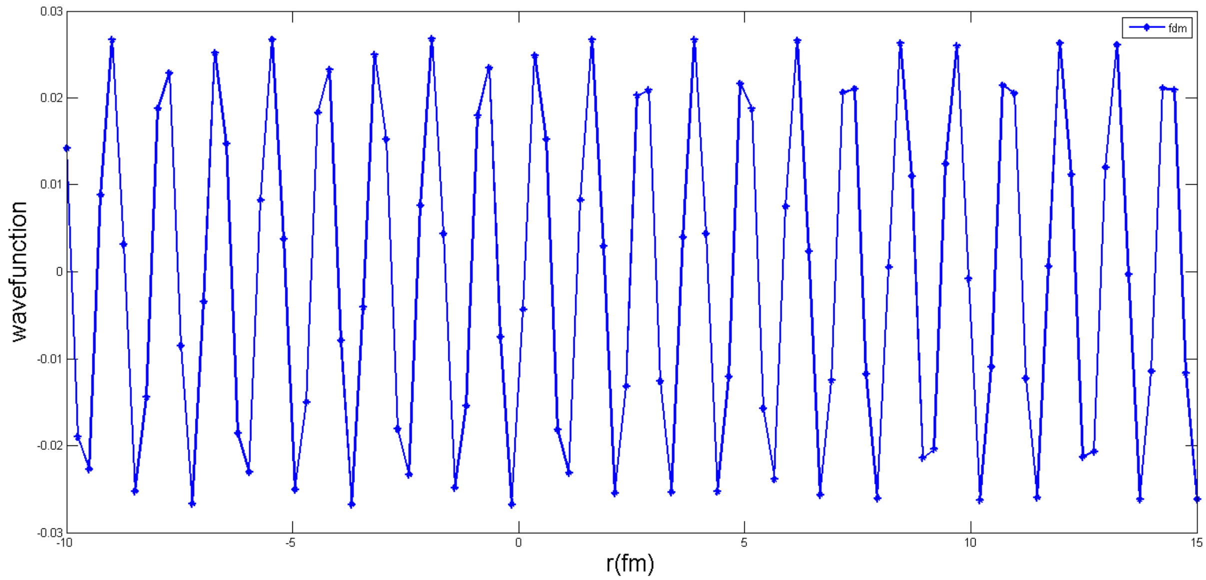

Figure 45: Wave function vs. r(fm) for $W_0 = 50\ MeV, l = 0, a = 0.65\ fm, V_0 = 47.78\ MeV, R_0 = 4.9162\ fm, E = -0.04\ eV$

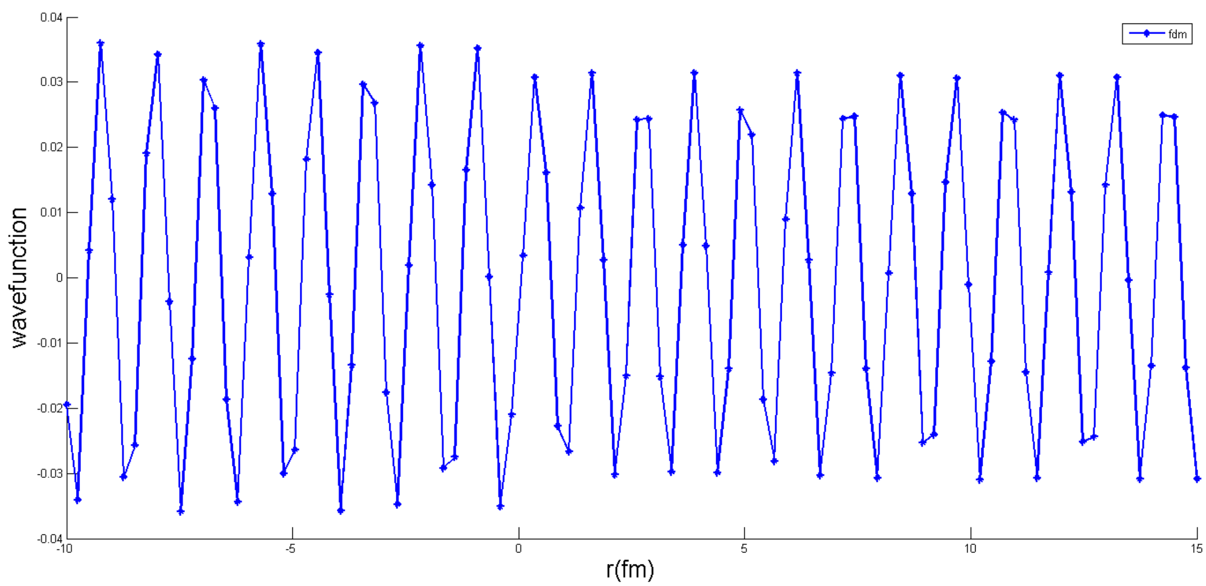

Figure 46: Wave function vs. r(fm) for $W_0 = 50\ MeV, l = 1, a = 0.65\ fm, V_0 = 47.78\ MeV, R_0 = 4.9162\ fm, E = -0.04\ eV$

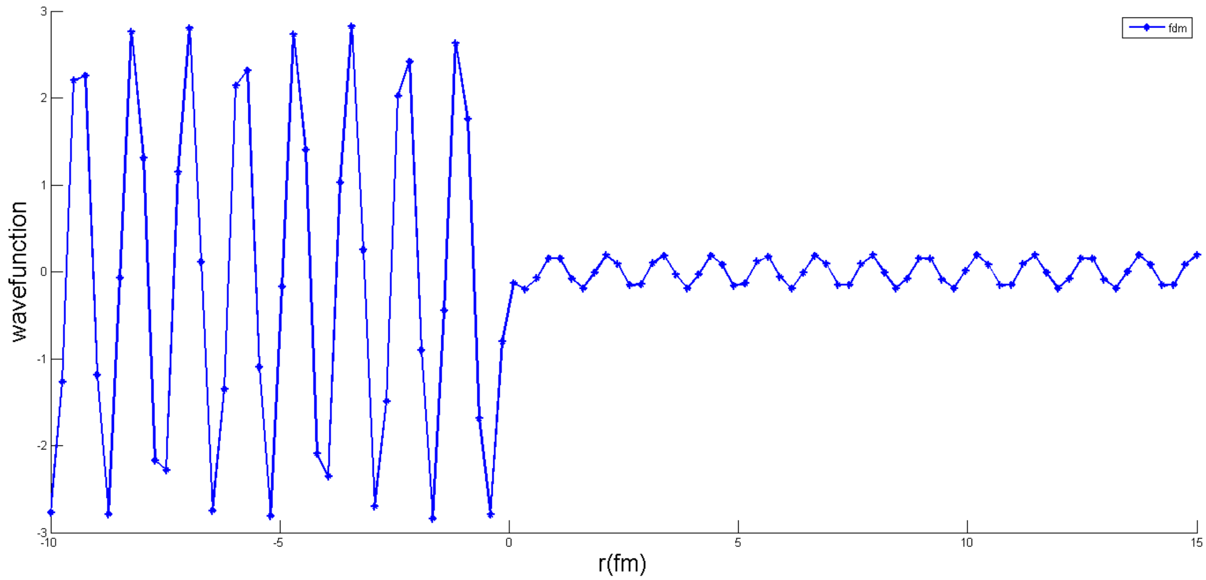

Figure 47: Wave function vs. r(fm) for $W_0 = 50\ MeV, l = 2, a = 0.65\ fm, V_0 = 47.78\ MeV, R_0 = 4.9162\ fm, E = -0.04\ eV$

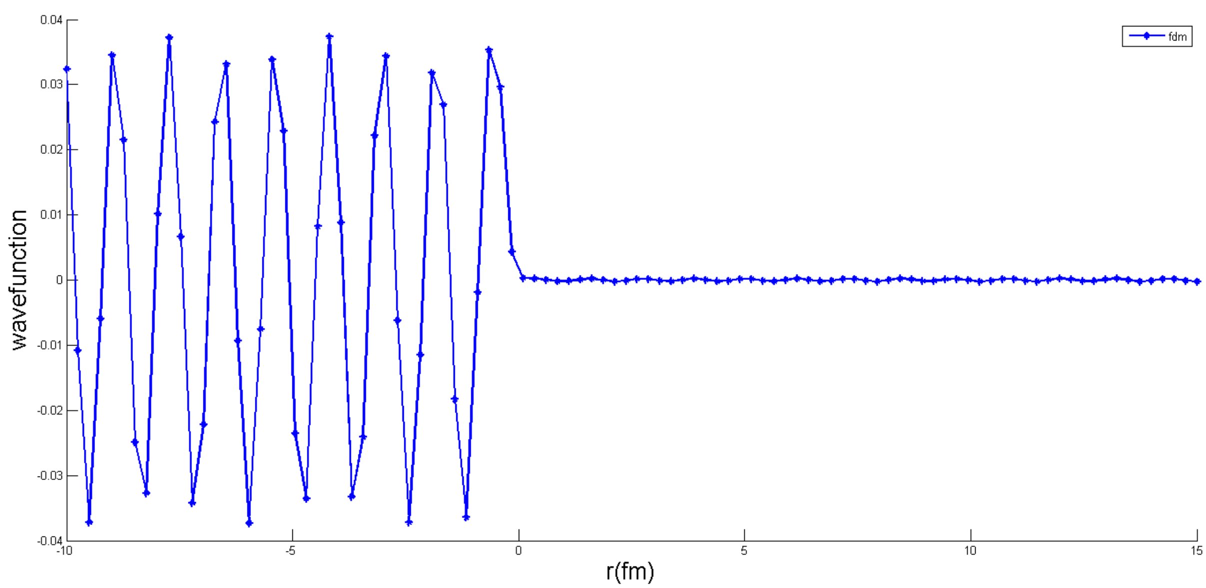

Figure 48: Wave function vs. r(fm) for $W_0 = 50\ MeV, l = 3, a = 0.65\ fm, V_0 = 47.78\ MeV, R_0 = 4.9162\ fm, E = -0.04\ eV$

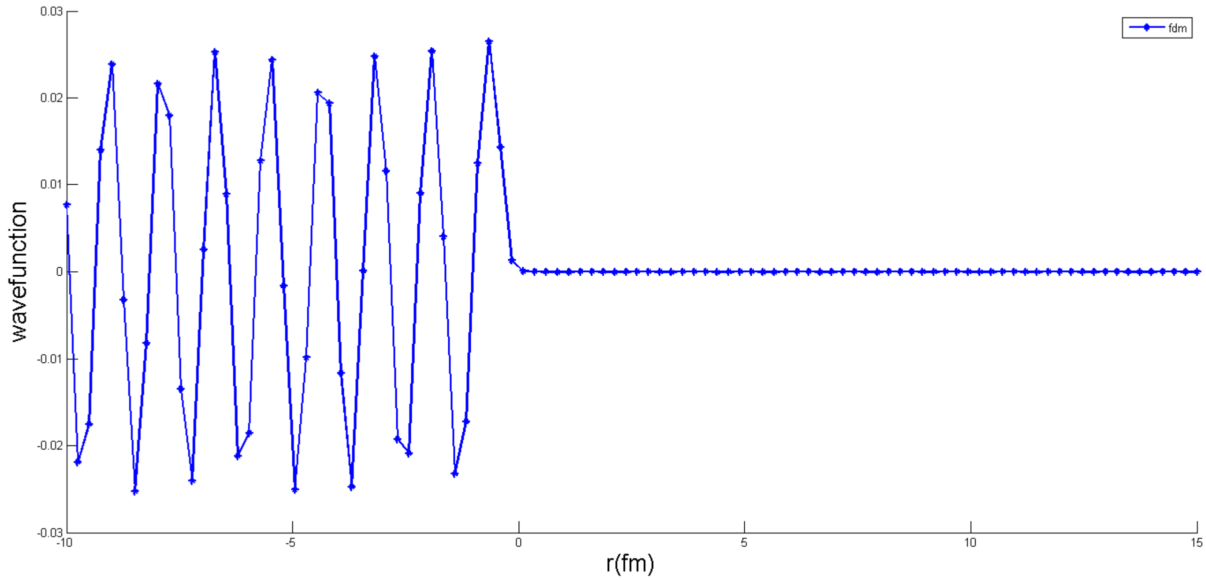

Figure 49: Wave function vs. r(fm) for $W_0 = 50\ MeV, l = 4, a = 0.65\ fm, V_0 = 47.78\ MeV, R_0 = 4.9162\ fm, E = -0.04\ eV$

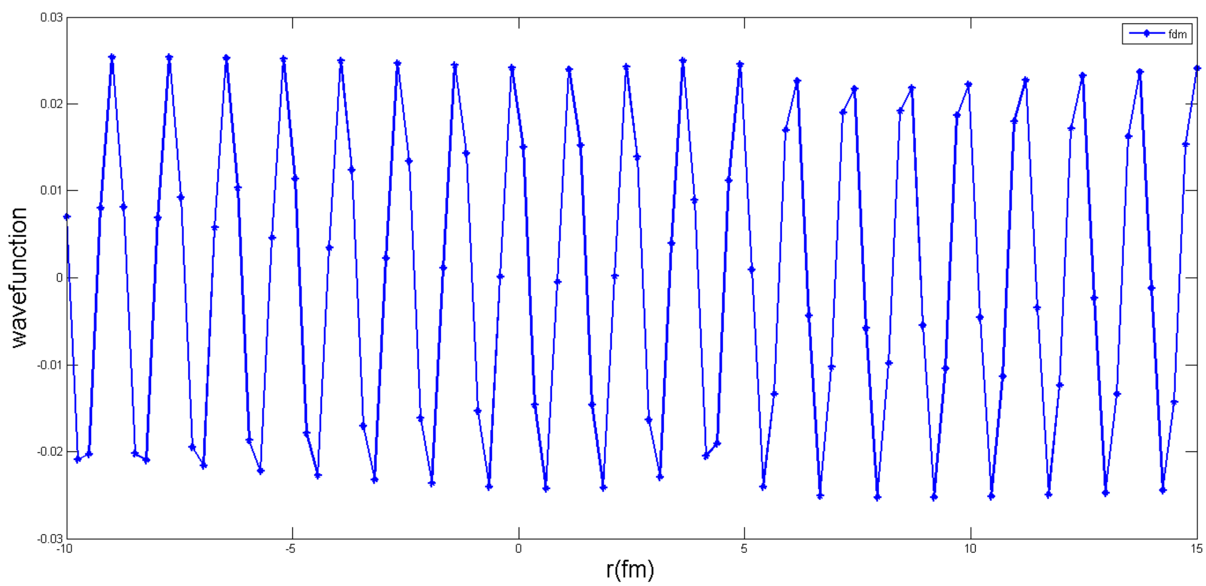

Figure 50: Wave function vs. r(fm) for $W_0 = 50\ MeV, l = 0, a = 0.65\ fm, V_0 = 47.78\ MeV, R_0 = 4.9162\ fm, E = -0.02\ eV$

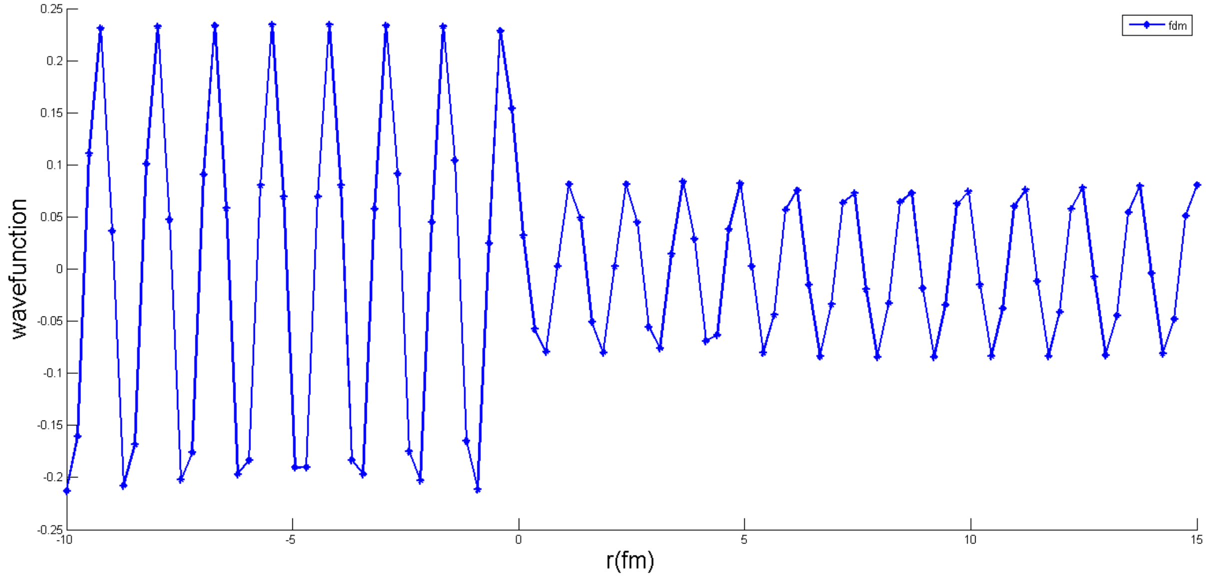

Figure 51: Wave function vs. r(fm) for $W_0 = 50\ MeV, l = 1, a = 0.65\ fm, V_0 = 47.78\ MeV, R_0 = 4.9162\ fm, E = -0.02\ eV$

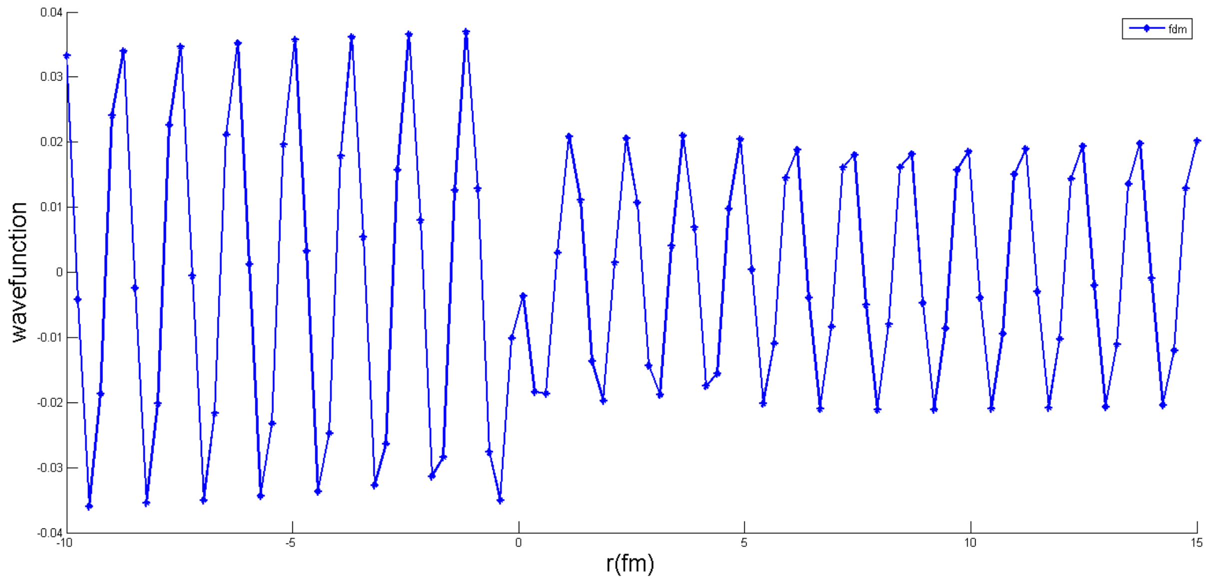

Figure 52: Wave function vs. r(fm) for $W_0 = 50\ MeV, l = 2, a = 0.65\ fm, V_0 = 47.78\ MeV, R_0 = 4.9162\ fm, E = -0.02\ eV$

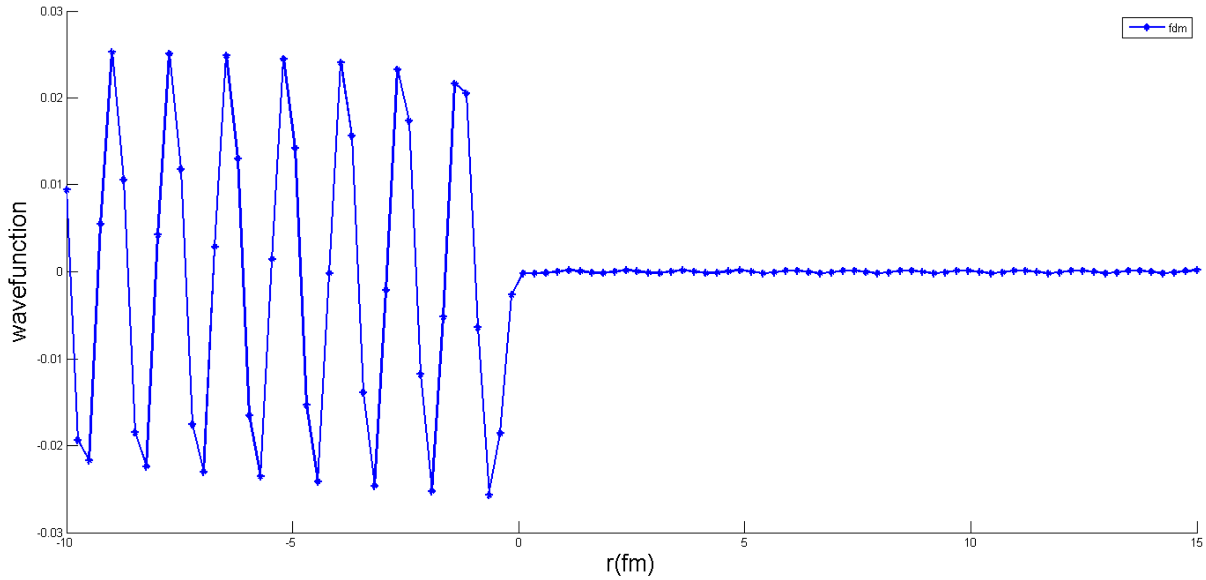

Figure 53: Wave function vs. r(fm) for $W_0 = 50\ MeV, l = 3, a = 0.65\ fm, V_0 = 47.78\ MeV, R_0 = 4.9162\ fm, E = -0.02\ eV$

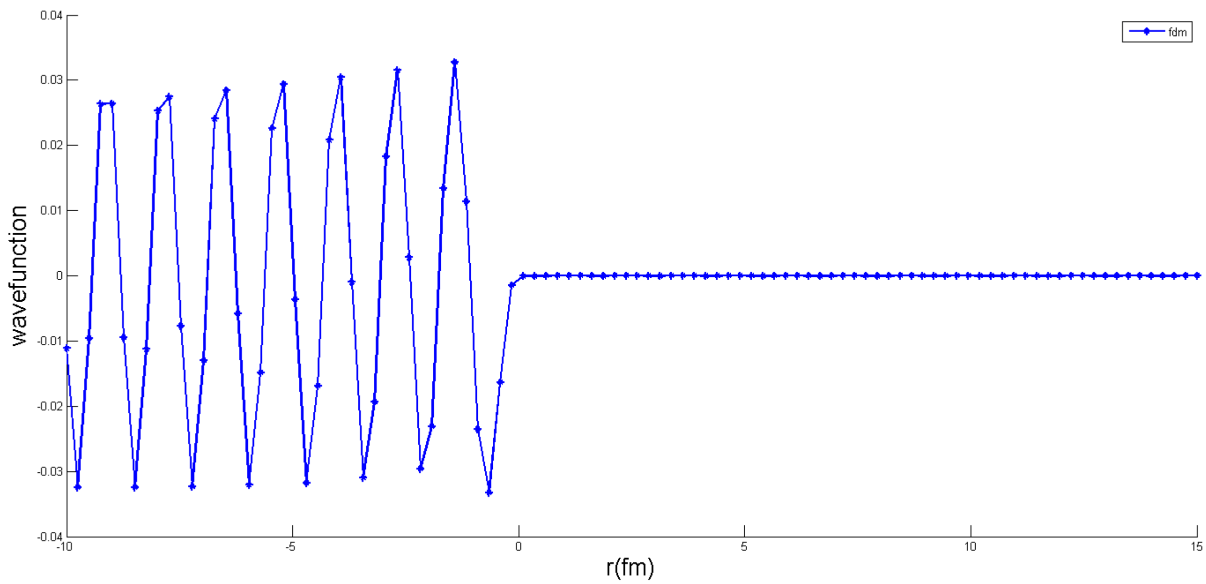

Figure 54: Wave function vs. r(fm) for $W_0 = 50\ MeV, l = 4, a = 0.65\ fm, V_0 = 47.78\ MeV, R_0 = 4.9162\ fm, E = -0.02\ eV$

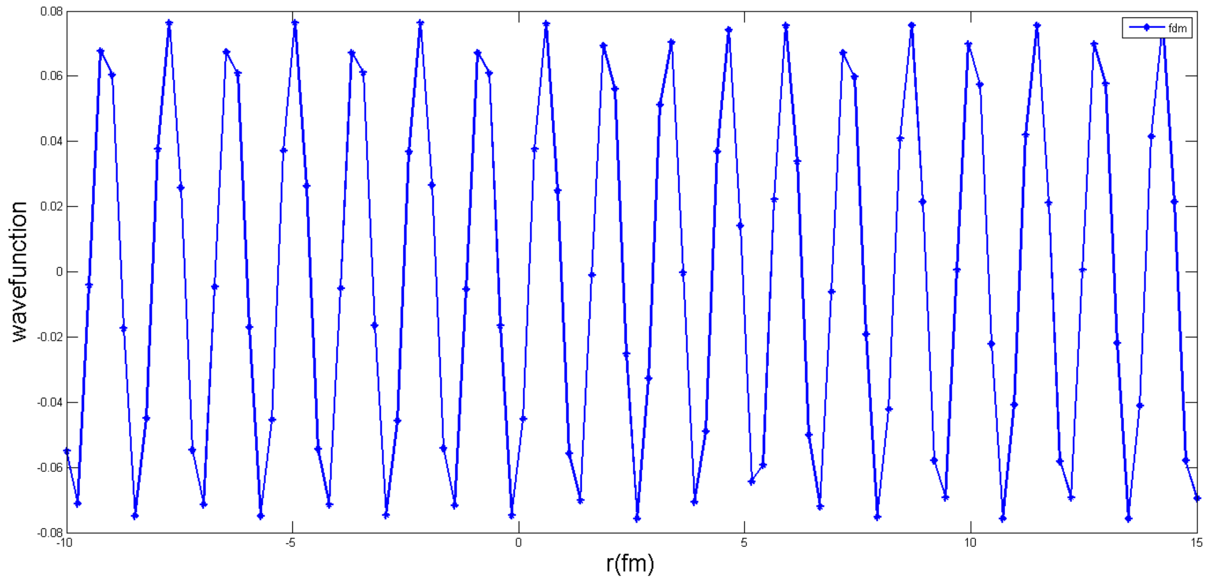

Figure 55: Wave function vs. r(fm) for $W_0 = 50\ MeV, l = 0, a = 0.65\ fm, V_0 = 47.78\ MeV, R_0 = 4.9162\ fm, E = -0.005\ eV$

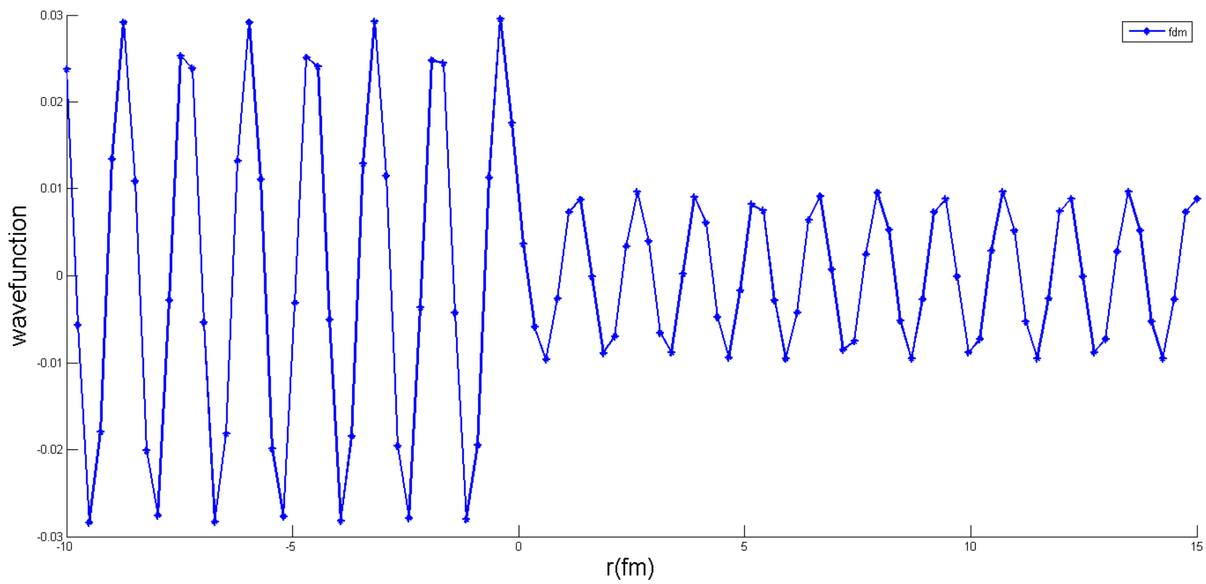

Figure 56: Wave function vs. r(fm) for $W_0 = 50\ MeV, l = 1, a = 0.65\ fm, V_0 = 47.78\ MeV, R_0 = 4.9162\ fm, E = -0.005\ eV$

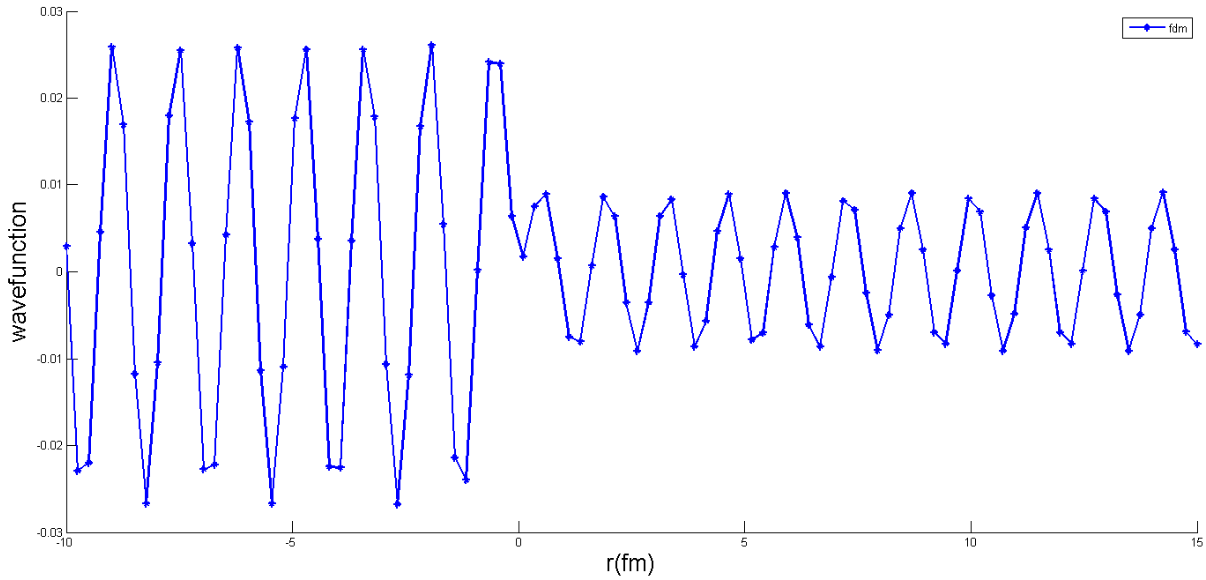

Figure 57: Wave function vs. r(fm) for $W_0 = 50\ MeV, l = 2, a = 0.65\ fm, V_0 = 47.78\ MeV, R_0 = 4.9162\ fm, E = -0.005\ eV$

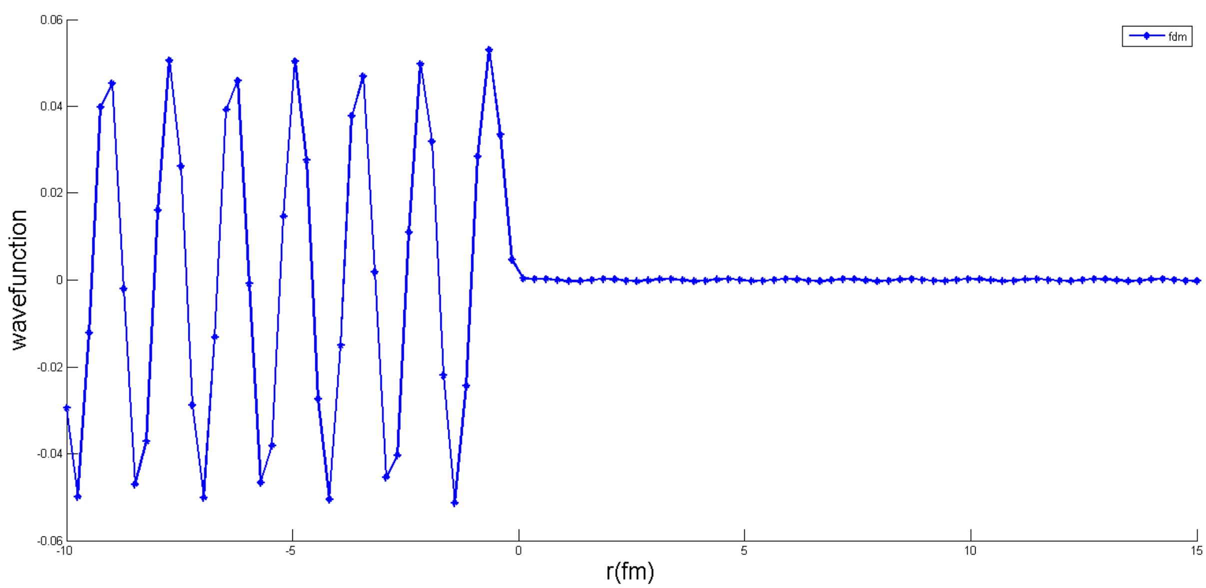

Figure 58: Wave function vs. r(fm) for $W_0 = 50\ MeV, l = 3, a = 0.65\ fm, V_0 = 47.78\ MeV, R_0 = 4.9162\ fm, E = -0.005\ eV$

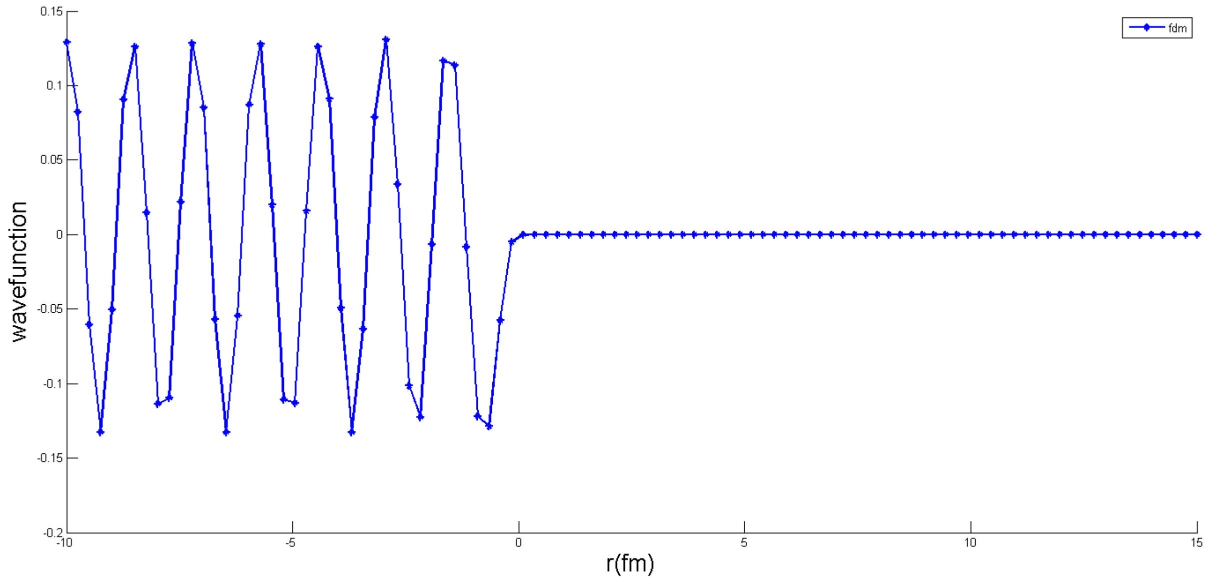

Figure 59: Wave function vs. r(fm) for $W_0 = 50\ MeV, l = 4, a = 0.65\ fm, V_0 = 47.78\ MeV, R_0 = 4.9162\ fm, E = -0.005\ eV$

B. Transmission Coefficient for neutron-Fe-56 interaction

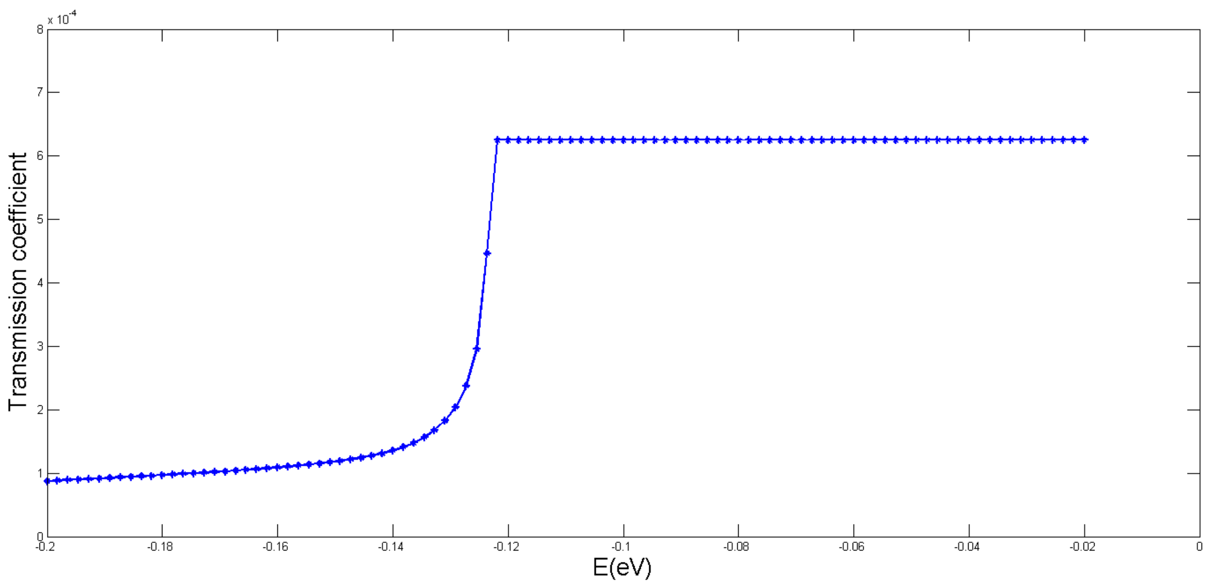

Figure 60: Transmission coefficient vs. E(eV) for energies of the incident neutron from $-0.2\ to - 0.02\ eV, l = 0$.

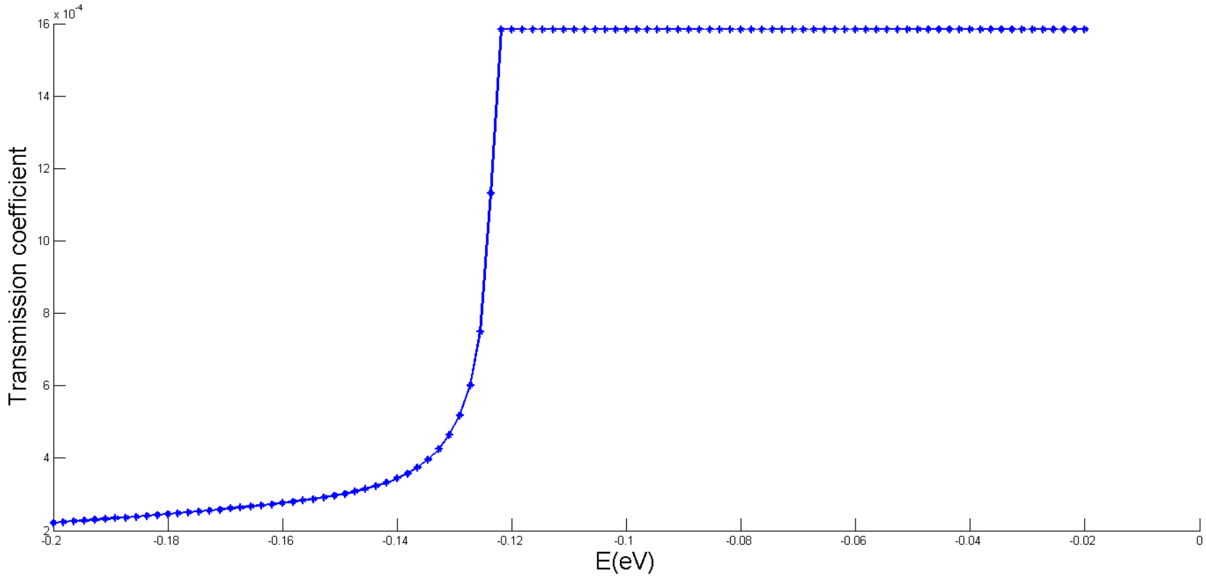

Figure 61: Transmission coefficient vs. E(eV) for energies of the incident neutron from $-0.2\ to - 0.02\ eV, l = 1$.

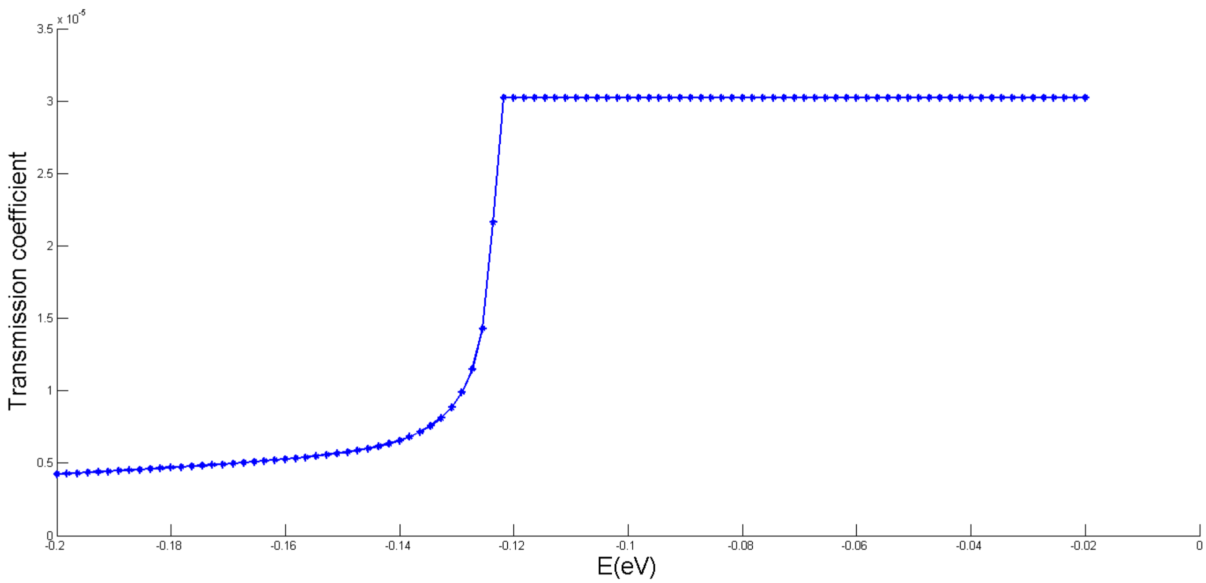

Figure 62: Transmission coefficient vs. E(eV) for energies of the incident neutron from $-0.2\ to - 0.02\ eV, l = 2$.

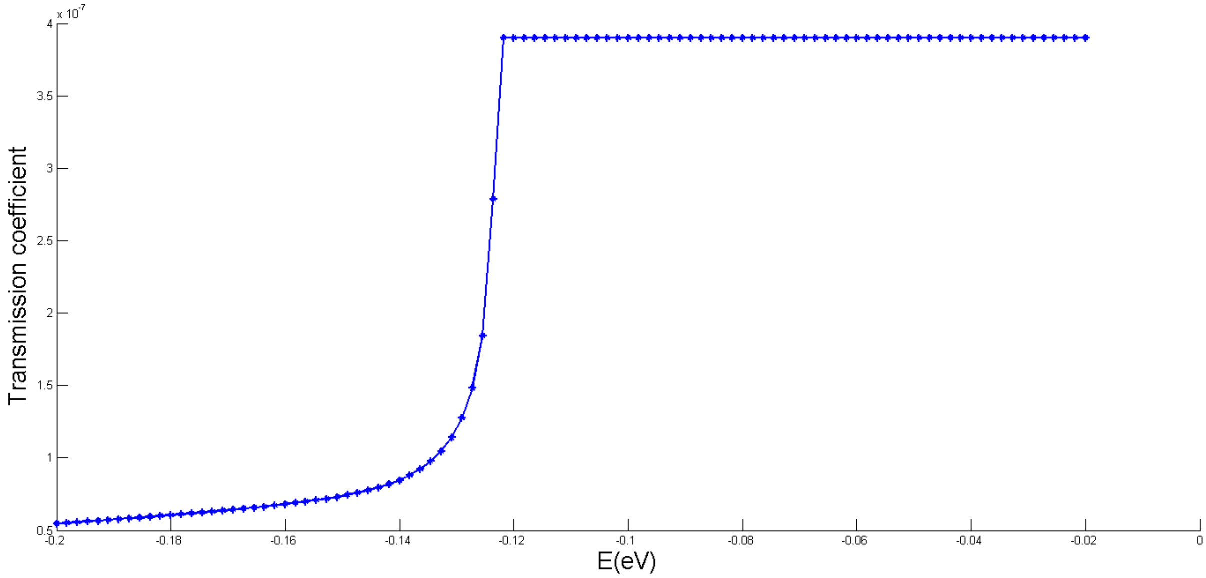

Figure 63: Transmission coefficient vs. E(eV) for energies of the incident neutron from $-0.2\ to - 0.02\ eV, l = 3$.

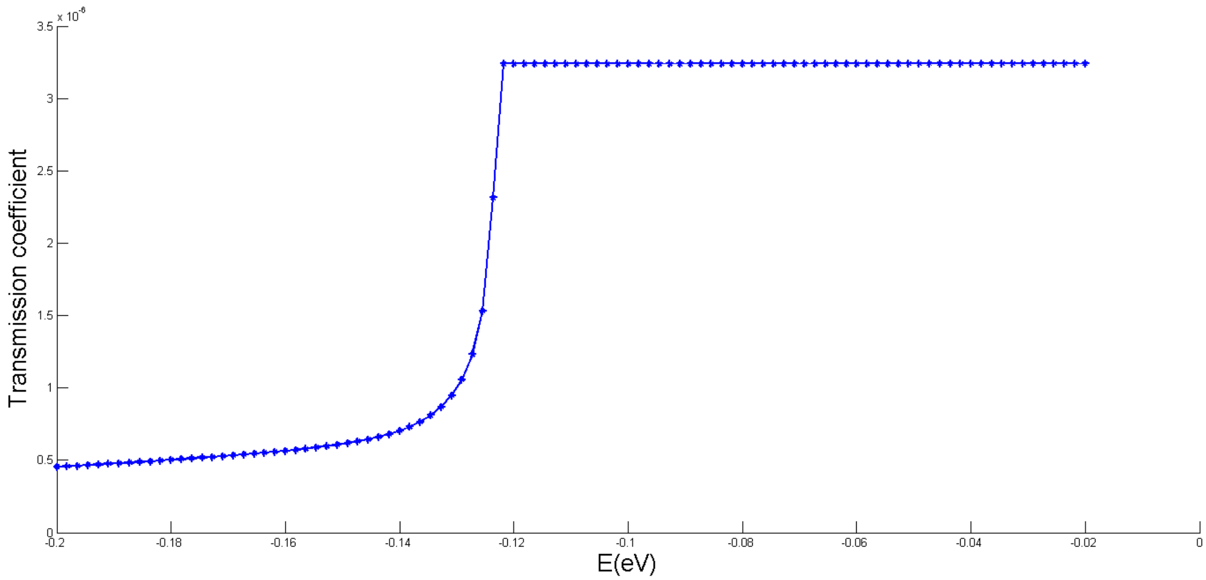

Figure 64: Transmission coefficient vs. E(eV) for energies of the incident neutron from $-0.2\ to - 0.02\ eV, l = 4$.

IV. DISCUSSION

The results from the plots in figure: 6-59 shows the typical simulation of Schrodinger equation with modified Woods-Saxon potential for, $W_0 = 50\ MeV$,$a = 0.65\ fm$,$V_0 = 47.78\ MeV$, $R_0 = 4.9162\ fm$ where V_0 and W_0 represent the depths of the potential well, R_0 and a are the radius of the potential and width of the surface diffuseness respectively. The results show the behavior of the wavefunction of the projected neutron as it tunnels through the barrier at different angular momenta $l = 0, 1, 2, 3, 4$ with various energies of the projected neutron.

Figure: 5, 10, 15, 20, 25, 30, 35, 40, 45 and 50; shows that for angular momentum $l = 0$, corresponding to the ground state of a standing half-wavefunction, the transmitted wave of the projected neutron penetrates the potential barrier after tunneling and does not attenuate or reduce in intensity. It is evident that for $l = 0$, the wave does not lose its energy after interacting with the Fe-56 nucleus and tunneling through it.

Figure: 6 and 21 show that the amplitude of the projected neutron increases as it tunnels through the barrier for $l = 1$. This is due to the difference in wave speed and particle (neutron) speed [23]. When the particle speed is small as compare to wave speed, the transmitted amplitude can be larger than the incident amplitude. Thus, it appears that the transmitted wave has larger amplitude and is moving faster, obscuring the correct explanation, that it has a smaller particle speed to compensate for the larger amplitude.

The results from figures: 11, 16, 26, 31, 41, 46, 51 and 56 show that for $l = 1$, the wave of the projected neutron in region I, there exists a maxima and minima due to the interference between incident and reflected waves of equal amplitude. At the boundary,$r = 0\ fm$, the wave attenuates within the barrier and joins smoothly to its constant value in region III. That is, when the projected neutron undergoes elastic collisions, energy is lost to the target and the neutron slows down. The energy losses are a relatively large fraction of the initial energy.

The results from figures: 7, 12, 17, 22, 27, 32, 37, 42, 47 and 52 show that the wave function of the projected neutron loses its energy at the potential barrier wall; $r = 0\ fm$ for $l = 2$. This shows that at higher angular quantum numbers, there is more rotational motion in the form of transverse vibrations of the projected neutron and hence its energy is distorted and so its wave function attenuates.

Results from figures: 8, 13, 18, 23, 28, 33, 38, 43, 48 and 53 show that the wave function of the projected neutron loses its energy drastically at the potential barrier wall; $r = 0\ fm$ for $l = 3$. This also, means that at higher angular quantum numbers, there is more rotational motion in the form of transverse vibrations of the projected neutron and hence its kinetic energy is distorted and so its wave function attenuates.

The results in Figure: 9, 14, 19, 24, 29, 34, 39, 44, 49 and 54 are similar to the results for $l = 3$. The results show that the wave function of the projected neutron loses its energy drastically at the potential barrier wall; $r = 0\ fm$ for $l = 4$. This show that at higher angular quantum numbers, there is more rotational motion in the form of transverse vibrations of the projected neutron and hence its energy is distorted and so its wave function attenuates and, in most cases, the wave dies off due to the presence of the potential barrier.

The results of the eigenfunctions for angular quantum number $l = 0$ obtained, is in agreement with the work by [24]. However, in their method, the boundary conditions were set at zero and the transmitted wave was not taken into consideration. The parameters used were also similar for a neutron-Fe-56 interaction ($V_0 = 47.78\ MeV$, $W_0 = -100\ to\ 100MeV$, $R_0 = 4.9162\ fm$, $a = 0.65\ fm$, and $r_0 = 1.285\ fm$).

The tendency of the projected neutron, upon interaction with the Fe-56 nucleus to penetrate or tunnel through the barrier is given in Eq. 27. The results of figures: 60, 61, 62, 63 and 64 show the variation in energies of the projected neutron as it encounters the Fe-56. The results show that the projected neutron can tunnel through the barrier even with energies of the projected neutron being less than the energy of the barrier contrary to the classical expectation. In each of the figures, the transmission coefficient attains saturation at an energy approximately equal to $E_s = -0.1309\ eV$. This implies that no projected neutron energy greater than E_s will, hence the transmission. The E_s value may serve as an experimental guide (given the barrier parameters as shown in the figures) in neutron- $Fe - 56$ scattering experiments particularly in elastic regime.

The transmission coefficient is significantly small. This is as a result of the potential (Woods-Saxon potential l) within the $Fe - 56$. The neutron on interacting with Fe-56 can be absorbed or reflected by Fe-56 [4].

Also, the results of figures: 60, 61, 62, 63 and 64 show the effects of angular momentum quantum numbers l on transmission coefficient for the neutron-Fe-56 interaction. The results indicate that as the angular mom entum quantum number l increases, the transmission coefficient decreases. This means that at higher angular momentum quantum numbers, there is more rotational energy $E_r \approx \sqrt{l(l+1)}\hbar$ in the form of transverse vibrations of the projected neutron which is at the expense of the neutron kinetic energy hence the neutron wave functions attenuate increasingly.

V. SUMMARY AND CONCLUSSION

The numerical solution of the problem was implemented by the discretization of the radial part of the Schrödinger equation using central finite difference method. This discretization method was used to discretize the radial part of the Schrodinger equation with modified Woods-Saxon potential. In order to demonstrate a propagating particle (the projected neutron) through a potential barrier, boundary conditions were assumed. The boundary conditions at the left and right-side boundaries were assumed for a projected neutron, to be at equilibrium with uniform potential energy. The solution starts with assuming a plane wave. The potential barrier for the neutron-Fe-56 interaction was in the region $r \in [0, 10]$fm). The plane wave of the projected neutron from the left was considered in the region, $r \in [-10, 0]$fm) while at the right it was considered to be in the region, $r \in [10, 15]$fm). These conditions were matched at the two boundaries and the resulting eigensystems of equations were presented in matrix form. In solving these eigensystems, the Jacobi method was applied to transform the eigensystems to a diagonalize coefficients matrix.

A Matrix Laboratory (MATLAB) computer code (shown in Appendix A) was used to solve for the eigenfunctions using guessed energies of the projected neutron. The guessed energy values for the projected neutron were considered based on the nature of the modified Woods-Saxon Potential.

For angular quantum number $l = 0$, the transmitted wave of the projected neutron, after tunneling does not attenuate. It is evident that for $l = 0$, the wave does not lose its energy after interacting with the Fe-56 nucleus. For $l = 1$, the wave of the projected neutron in region I, shows that there exists a maxima and minima due to the interference between incident and reflected waves of equal amplitude. At the boundary,$r = 0\ fm$, the wave attenuates within the barrier and joins smoothly to its constant value in region III. That is, when the projected neutron undergoes elastic collisions, energy is lost to the target and the neutron slows down. The energy losses are a relatively large fraction of the initial energy. Also, some eigenfunctions shows that amplitude of the projected neutron increases as it tunnels through the barrier for $l = 1$. This may be attributed to the difference in wave speed and particle (neutron) speed. When the particle speed is small as compared to wave speed, the transmitted amplitude is larger than the incident amplitude. Thus, it appears that the transmitted wave has larger amplitude and is moving faster, obscuring the correct explanation, that it has a smaller particle speed to compensate for the larger amplitude. The wave function of the projected neutron loses its energy drastically at $r = 0\ fm$ for $l = 2$, $l = 3$ and $l = 4$. This shows that at higher angular quantum numbers, there are high circular vibrations of the projected neutron and its wave function attenuates and, in most cases, the wave dies off due to the presence of the potential barrier.

To demonstrate quantum tunneling, current conservation was applied. The relationship between the transmission coefficient and energy of the projected neutron was solved and simulated using MATLAB computer code (shown in appendix B).

The results from the plot of the transmission coefficient and energies of the projected neutron show that the projected neutron can tunnel through the barrier even with energies of the projected neutron is less than the energy of the barrier.

In conclusion, the eigenfunctions and the transmission coefficient for a neutron-Fe-56 were simulated and the results are in agreement with a tunneling probability of a particle incident on a potential barrier even though the energy of the particle is less than the energy of the barrier. Also, it was found that the transmission coefficient attains saturation at an incident energy of about $-0.1309\ eV$.

Acknowledgment

I am grateful to God for the good health and well-being that were necessary to complete this research work.

I wish to extend my sincere gratitude to my supervisor, Prof. I. M. Echi, who has the mind of an expert. He patiently instructed and encouraged me to think big and not to give up when all seemed not to be working out. Without his unique assistance, the goal of this thesis would never have been realized.

I would also like to acknowledge Prof. A. D. Onoja as the co-supervisor of this thesis, and I am gratefully indebted to his very valuable comments on this thesis.

I take this opportunity to express gratitude to Head of Department of Physics, Dr. I. Ahemen, all of the Department of Physics lecturers and the entire staff for their help and support.

I am also grateful to Dr. E. Tikyaa, lecturer, in the Department of Physics. I am extremely thankful and indebted to him for sharing expertise, and sincere and valuable guidance and encouragement extended to me.

I must express my very profound gratitude to my parents, Mr. & Mrs. Ormin Akaa and to my brother and sisters; Dr. K. Raphael, Mrs. Mbanan Elizabeth and Miss. Zungwen Doris for providing me with unfailing support and continuous encouragement throughout my years of study and through the process of researching and writing this thesis. This accomplishment would not have been possible without them.

Lastly, I would like to thank my amazingly supportive friends (Mic, Nico, Ayamila and Abigail) and colleagues for all your various supports.

APPENDIX A: MATLAB code for solution of Radial Schrodinger Equation

```
clc;clf;clear all;
a=0.65;V0=47.78;R0=4.9162;W0=50;l=0;
m=940.35; a1=-10;a2=10;hbar=197.3; E=-0.16;
rmin=-10;rmax=15;n=100;
r=linspace(rmin,rmax,n);
dr=r(2)-r(1);
%effective potential
V=(-(V0*(1+exp(r-R0)/a).^-1))+(W0*(1+exp(r-R0)/a).^-2)+(l*(l+1)*r.^-2);
%wavenumber within the potential barrier
k=(sqrt(2*m*(E)))/hbar;
%alfa
t=hbar^2/(2*m*dr);
d=-2.0795;
z=E-V-2*t+t*exp(1i*k*a1);
%Building up the matrix
A=zeros(n,n);
A(1:1+n:n*n)=z;
A(n+1:1+n:n*n)=t;
A(2:1+n:n*n-n)=t;
%RHS
B=zeros(n,1);
B(1)=d;
B(2:n-1)=0;
B(n)=0;
%Solving the system
U=A\B;
plot(r,(U),'-*','linewidth',2);
xlabel('r(fm)','fontsize',20);
ylabel('wavefunction','fontsize',20)
grid off;
legend('fdm');
```


APPENDIX B: MATLAB code for transmission coefficient

```
clc;clf;clear all;
a=0.65;V0=47.78;R0=4.9162;W0=50;l=0;
m=940.35; a1=-10;a2=10;hbar=197.3;
n=100;
rmin=-10;rmax=10;
r=linspace(rmin,rmax,n);
dr=r(2)-r(1);
Emin=-0.2;Emax=-0.02;
E=linspace(Emin,Emax,n);
dE=E(2)-E(1);
%value of Un
U(n)=-0.025;
V=(-(V0*(1+exp(r-R0)/a).^-1))+(W0*(1+exp(r-R0)/a).^-2)+(l*(l+1)*r.^-2);
%wavenumber to the right
k_R=(sqrt(2*m*(E-V)))/hbar;
%wavenumber to the left
k_L=(sqrt(2*m*(E)))/hbar;
%T is the transmission probability
T=(k_R/k_L)*((U(n)).^2)*exp((2*k_R*1i*a2));
t=abs(T);
plot(E,t,'-*','linewidth',2);
xlabel('E(eV)','fontsize',20);
ylabel('Transmission coefficient','fontsize',20)
```

References

[1] Abbas T., and Slewa L., (2015). Transmission line method (TLM) measurement of (metal/ZnS) contact resistance. International Journal of Nanoelectronics and Materials 8 (2015) 111-120

[2] Akaninyene D. A., Ita O. A., Ikot A. N., Elham M., Saber Z., and Hassan H., (2015). Analytical solutions of Schrödinger Equation with new solvable Potential Family via Nikiforov-Uvarov (NU) method. Annales Universitatis Mariae Curie - Sklodowska Lublin– Polonia Vol. LXX Sectio AAA (2015).

[3] Badalov V. H., Ahmadov H. I., and Ahmadov A. I., (2008). Analytical solutions of the Schrodinger equation with the Woods-Saxon Potential for arbitrary l state. International Journal of Modern Physics E Vol. 18, No. 3 (2009) 631-641

[4] Badalov V. H., Baris B., and Uzun K., (2017). Bound states of the D-dimensional Schrodinger equation for the generalized Woods-Saxon potential. arXiv:1711.10322v1 [nucl-th] 24 Nov 2017.

[5] Benjamin O. T., (2019). Finite Difference Solution of the Schrodinger Equation. Extracted from: Modern Physics Medium¬¬_1619633061414.pdf.

[6] Brian C. H., (2013). Quantum Theory for Mathematics. Department of Mathematics, University of Notre Dame Notre Dame, IN, USA. ISBN 978-1-4614-7116-5 (eBook) DOI: 10.1007/978-1-4614-7116-5

[7] Capak M., and Gonul B., (2016). Remarks on the Woods Saxon potential. Modern Physics Letters A Vol. 31, No. 23 (2016) 1650134. DOI: 10.1142/S0217732316501340

[8] Diego A. A., (2020). Macroscopic quantum tunneling and Quantum many-body dynamics in Bose-Einstein condensates. A thesis submitted to the Faculty and the Board of Trustees of the Colorado School of Mines in partial fulfillment of the requirements for the degree of Doctor of Philosophy (Physics).

[9] Ervin B. P., (2009). Interaction of Neutrons with Matter. Radiation Physics for medical Physicists pp 429-449. https://doi.org/10.1007/978-3-642-00875-79

[10] Farhang L., and Ali M., (2020). Transfer-matrix formulation of the scattering of electromagnetic waves and broadband invisibility in three dimensions. arXiv:1901.09093v4 [quant-ph] 4 Apr 2020

[11] Guan-Ru F., Yao L., Liang H., Fei-Hao Z., and Gui-Lu L., (2013). Experimental simulation of quantum tunneling in small systems. Sci. Rep. 3, 2232; DOI:10.1038/srep02232 (2013).

[12] Harpinder Kaur, Khushpreet Kaur, (2012). Convergence of Jacobi and Gauss-Seidel Method and Error Reduction Factor. Journal of Mathematics. ISSN: 2278-5728 Volume 2, Issue 2 (July-Aud 2012), pp 20-23

[13] Hartman T. E., (1962). Tunneling of a wave packet. Journal of applied Physics 33(12), 3427-3433 (1962).

[14] Hassanabadi H., Yazarloo B. H., Zarrinkamar S., and Solaimani M., (2012). Approximate Analytical Versus Numerical Solutions of Schrodinger Equation Under Molecular Hua Potential. International Journal of Quantum Chemistry. DOI: 10.1002/qua.24064

[15] Helmut Schober (2014). An introduction to the theory of nuclear neutron scattering in condensed matter. Journal of Neutron Research 17 (2014) 109–357. DOI: 10.3233/JNR-140016

[16] Herman et al., (2018). Evaluation of Neutron Reactions on Iron Isotopes for CIELO and ENDF/B-VIII.0. Nuclear Data Sheets 148 (2018) 214–253 https://doi.org/10.1016/j.nds.2018.02.004

[17] Ikot A. N., Akpabio L. E., and Umoren E. B., (2010). Exact Solution of Schrödinger Equation with Inverted Woods-Saxon and Manning-Rosen Potential. Journal of Scientific Research 3 (1), 25-33 (2011). doi:10.3329/jsr.v3i1.5310

[18] Kelvin S., and Guy B., (2017). Simulations in quantum tunneling. American Journal of Physics 85, 763 (2017). doi: 10.1119/1.4991367

[19] Kevin-Alexander B., (2018). Numerical simulations of neutron scattering cross sections for heavy nuclei. A bachelor thesis submitted to the department of Physics, Karl-Franzens-Universitat Graz, Austria.

[20] Kouichi H., and Noboru N., (2012). Subbarrier Fusion Reactions and Many-Particle Quantum Tunneling. Progress of Theoretical Physics, Vol. 128, No. 6, December 2012

[21] Lin G., ZhiHong L., HuiBin S., DanY. P., Bing G., YunJu L., Jun S., ShengQuan Y., ErTao L., YouBao W., Gang L., ZhiYu H., XinYue L., DongHui L., TianLi M., ChangJin P., YangPing S., Yi S., Sheng Z., Yong Z., and WeiPing L., (2017). Parametrization of woods-saxon potential for heavy-ion systems. Sci. China-Phys. Mech. Astron. Vol. 60 No. 8: 082013 (2017), doi: 10.1007/s11433-017-9061-5

[22] Loren J., David L. C., and Etienne T., (2011). Numerical Resolution of the Schrödinger Equation. École Normale Supérieure de Lyon, Master Sciences de la Matière 2011. http://perso.ens-lyon.fr/etienne.thibierge/ana_num

[23] McKagan S. B, Perkins K. K, and Wieman C. E. (2008). A Deeper Look at Student Learning of Quantum Mechanics: The Case of Tunneling. DOI: http://dx.doi.org/10.1103/PhysRevSTPER.4.020103.

[24] Mirzaei M. A. V., Hosseini R. A., Javad. M., and Rahim K. K., (2013). Numerical solution of the Schrödinger equation for types of Woods-Saxon potential. Faculty of Physics, Shahid Bahonar University, P.O. Box 76175, Kerman, Iran.

[25] Neill L., (2001). Numerical Solutions of Schrodinger's Equation. Extracted from: https://www1.itp.tu-berlin.de/brandes/public_html/qm/qv3.pdf

[26] Ning W., and Werner S., (2008). Quasi-elastic scattering and fusion with a modified Woods-Saxon potential. Physical Review C 78, 014607 (2008). DOI:10.1103/PhysRevC.78.014607

[27] Sanjib M., and Debnath S., (2010). Eigen spectra for Woods-Saxon plus Rosen-Morse potential. Lat. American Journal of Physics Education. Vol. 4, No. 3, Sept. 2010. ISSN 1870-9095

[28] Schroeder D. V., (2020). Notes on Quantum Mechanics. Weber State University.

[29] Sebawe M. A., and Eleuch H., (2014). Exact analytic solutions of the Schrödinger equations for some modified q-deformed potentials. A journal of applied science. https://doi.org/10.1063/1.4883296

[30] Sornborger, A. T., (2012). Quantum simulation of tunneling in small systems. Extracted from: Scientific Reports 2, 597(2012).

[31] Tarek M. A., Ahmed S., and Alahmadi A. N. M., (2018). Numerical Simulation of Tunneling Through Arbitrary Potential Barriers Applied on MIM and MIIM Rectenna Diodes. European Journal of Physics. 39;045402 (24pp).

[32] Tianrong Zhan, Xi Shi, Yunyun Dai, Xiaohan Liu and Jian Zi, (2013). Transfer matrix method for optics in graphene layers. Journal of Physics: Condensed Matter 25 (2013) 215301 (10pp).

[33] Toubiana A. J., Canto L.F., and Hussein M.S., (2017). Improved WKB approximation for quantum tunneling: Application to heavy-ion fusion. European Physics Journal. 53: 34. DOI 10.1140/epja/i2017-12225-6

[34] Towhiduzzaman Md., (2016). Performance Analysis of Continuity Equation and its Application. European Journal of Engineering Research and Science, Vol. 1, No.5 November 2016.

[35] Trixler, F (2013). "Quantum tunnelling to the origin and evolution of life". Current Organic Chemistry. 17 (16): 1758–1770. doi:10.2174/13852728113179990083. PMC 3768233. PMID 24039543.

[36] Wysin G. M., (2011). Probability Current and Current Operators in Quantum Mechanics. Department of Physics, Kansas State University, Manhattan, KS 66506-2601. http://www.phys.ksu.edu/personal/wysin